Weierstraß-Institut
für Angewandte Analysis und Stochastik
Leibniz-Institut im Forschungsverbund Berlin e. V.

The mathematics behind chimera states

Oleh E. Omel'chenko

submitted: November 28, 2017

Weierstrass Institute
Mohrenstr. 39
10117 Berlin
Germany
E-Mail: oleh.omelchenko@wias-berlin.de

The mathematics behind chimera states

Oleh E. Omel'chenko

Abstract

Chimera states are self-organized spatiotemporal patterns of coexisting coherence and in-coherence. We give an overview of the main mathematical methods used in studies of chimera states, focusing on chimera states in spatially extended coupled oscillator systems. We discuss the continuum limit approach to these states, Ott-Antonsen manifold reduction, finite size chimera states, control of chimera states and the influence of system design on the type of chimera state that is observed.

1 Introduction

Self-organization of complex systems lies at the heart of many studies in physics, chemistry, biology and social sciences. The key question is to understand how simple nearly identical agents coupled together can produce spontaneous collective order. An important example of this kind was discovered 15 years ago in coupled oscillator systems, when Kuramoto and Battogtokh showed [62] that structured patterns of coherence and incoherence can emerge from otherwise structureless oscillatory networks, and in particular that even in systems of identical oscillators some oscillators could exhibit coherent oscillations while others oscillated incoherently. This behavior was not expected and led Abrams and Strogatz to suggest [1] the name *chimera state* for this type of state.

The number of papers dealing with chimera states has grown drastically over the last decade demonstrating increasing interest in this topic. This paper is an attempt to collect together the most interesting (in the author's opinion) results, that form our present, still incomplete understanding of this spectacular dynamical phenomenon. In contrast to other reviews [128, 143, 179, 11] revealing mainly the phenomenology of chimera states, here we try to analyze their mathematical nature and describe the mathematical tools used to study them. We focus mainly on chimera states that appear as coherence-incoherence patterns in spatially extended systems of coupled oscillators. This is perhaps one of the most studied examples of chimera states, and it still remains far from completely understood.

The paper is organized as follows. In Section 2 we give an overview of typical examples of chimera states observed in systems of non-locally coupled phase oscillators. In Section 3, we define a general spatially extended coupled oscillator system and write its continuum limit equation. We recall situations when this equation can be simplified by means of the Ott-Antonsen manifold reduction technique. Next we discuss examples of the continuum limit equation corresponding to different coupled oscillator models and outline a general bifurcation analysis scheme for chimera states. In Section 4, we survey finite size features of chimera states and methods of their statistical analysis. Then, in Section 5 we explain how chimera states can be controlled. Examples of unbounded oscillatory media and chimera-like states observed there will be discussed in Section 6. At the end of the paper, in Section 7 we give a brief overview of other mathematical models where chimera states or similar spatiotemporal patterns can be found. There we also discuss alternative definitions of chimera states. Finally, in Section 8 we formulate some concluding remarks.

2　Basic facts about chimera states

The prototype model where chimera states have been first reported is a ring of identical non-locally coupled phase oscillators $\theta_k(t) \in \mathbb{R}$ described by an ODE system

$$\frac{d\theta_k}{dt} = \omega_0 - \frac{2\pi}{N} \sum_{j=1}^{N} G_1\left(\frac{2\pi}{N}(k-j)\right) \sin(\theta_k(t) - \theta_j(t) + \alpha), \quad k = 1, \ldots, N. \tag{1}$$

Here, $\omega_0 \in \mathbb{R}$ is the natural frequency of the oscillators, $\alpha \in \mathbb{R}$ is the so-called *phase-lag* parameter and $G_1 : \mathbb{R} \to \mathbb{R}$ is an even non-constant 2π-periodic function, called below the *coupling function*. Obviously, periodicity of function G_1 imposes periodic boundary conditions at the oscillator array.

To explain the origin of the term *non-local* when referring to the coupling in Eq. (1) let us recall that all-to-all coupling between oscillators is usually referred to as *global* coupling, whereas coupling to a fixed number of first neighbours is referred to as *local*. According to this convention, the coupling in Eq. (1) is neither global (provided G_1 is non-constant!) nor local. Such coupling is traditionally called *non-local*. Of course, it can also be called non-global, but this name is much less popular.

In general, non-local coupling can be defined by any non-constant function G_1, however, most of the results for chimera states in Eq. (1) were obtained with one of the following coupling schemes.

(i)　2π-periodic extension of the exponential function [62]

$$G_1(x) = \frac{\kappa}{2} e^{-\kappa|x|} \quad \text{for} \quad |x| \le \pi, \tag{2}$$

where $\kappa > 0$ is its decay rate. This coupling function has a clear physical interpretation: it is the Green's function associated with the differential operator $-\partial_x^2 + 1$. Consequently, the corresponding non-local coupling reduces to a coupling via an auxiliary diffusive agent, see Section 7.1. In the continuum limit case ($N \to \infty$) this equivalence allows us to replace some integral operators, involved in the analysis of chimera states, by the corresponding differential equations.

(ii)　2π-periodic extension of the top-hat function [119, 170, 171]

$$G_1(x) = \begin{cases} (2\pi\sigma)^{-1} & \text{for} \quad |x| \le \pi\sigma, \\ 0 & \text{for} \quad |x| > \pi\sigma, \end{cases} \tag{3}$$

where $\sigma \in (0,1)$ is its coupling radius. This coupling function is the best choice for numerical simulations. Using it one can significantly optimize numerical integration of Eq. (1) without any restriction on the system size N.

(iii) Trigonometric function [1, 2, 121, 174]

$$G_1(x) = \frac{1}{2\pi}(A_0 + A_1 \cos x + A_2 \cos(2x)), \quad A_0, A_1, A_2 \in \mathbb{R}. \tag{4}$$

This coupling is called *balanced* for $A_0 = 0$ and *non-balanced* for $A_0 \ne 0$ and is convenient for bifurcation analysis of chimera states in the continuum limit, see Section 3.

Typical feature of Eq. (1) is its pronounced multistability. For example, numerical simulations of Eq. (1) with $\alpha \approx 0$ reveal so-called q-twisted states [168]

$$\theta_k(t) = \frac{2\pi q k}{N} + \Omega_q t + \text{const}, \qquad k = 1, \ldots, N,$$

where integer q counts the number of twists along the array and $\Omega_q \in \mathbb{R}$ is the constant angular speed of the oscillators, Fig. 1(a). In q-twisted states all oscillators are phase-locked, and we therefore call them *coherent* states. The state with $q = 0$ consists of fully synchronized oscillators and corresponds to *complete coherence*.
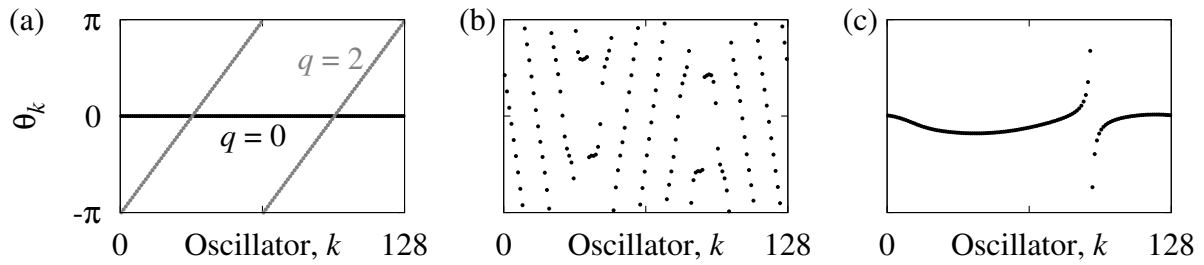

Figure 1: Coherent states in Eq. (1). (a) Two q-twisted states for the top-hat coupling (3) with $\sigma = 0.14$ and $\alpha = 0$. (b) Multi-twisted state for the same coupling and $\alpha = \pi$. (c) Coherent traveling wave solution for the trigonometric coupling (4) with $A_0 = 1$, $A_1 = 0.9$, $A_2 = 0$, and $\alpha = \pi/2 - 0.1$.

More complicated coherent states can also be found in Eq. (1). These are, for example, *multi-twisted* states [36], which have several spatial regions where oscillators are close to one or other twisted state, Fig. 1(b), or traveling wave solutions [33], which are quasiperiodic coherent solutions of Eq. (1), Fig. 1(c).

In spite of the abundance of simple coherent solutions, for some parameter values (usually $\alpha \approx \pi/2$) Eq. (1) can also exhibit dynamically more complicated and therefore more unexpected coherence-incoherence patterns, known as chimera states. Figure 2 shows two examples of such states: a chimera state with two anti-phase coherent regions, Fig. 2(c), and chimera state with a single coherent region, Fig. 2(d). Here, the term *coherent* region applies to a group of oscillators which are phase-locked, i.e. their velocities $\dot{\theta}_k(t)$ are almost identical for sufficiently long time and the corresponding phases $\theta_k(t)$ evolve synchronously, whereas the term *incoherent* region refers to the rest of the oscillators which drift with respect to each other and with respect to all coherent regions.

Another definition of coherence and incoherence based on the effective frequencies

$$\omega_{\text{eff},k} = \lim_{T \to \infty} \frac{1}{T} \int_0^T \dot{\theta}_k(t)dt$$

was recently suggested in [8, 13]. There a group of oscillators with equal $\omega_{\text{eff},k}$ is identified as coherent (note that, in general, there can be several such groups with different common frequencies), whereas the remaining oscillators with different $\omega_{\text{eff},k}$ are called incoherent. Unfortunately, this definition is non-universal and can be used in special cases only. For example, infinite time averages of the velocities $\dot{\theta}_k(t)$ cannot be used for the recognition of the chimera state in Fig. 2(c), because its coherent and incoherent regions change their position on the ring and because the chimera state is observed for a finite time span only and collapses eventually to another chimera state with a single coherent region, see Fig. 2(a). In Section 4 we will demonstrate that similar dynamical features (i.e. position wandering and collapse) are also inherent to the chimera state in Fig. 2(d). Therefore a definition of coherence and incoherence in terms of $\omega_{\text{eff},k}$ is meaningless for this chimera state as well.

The appearance of chimera states is most surprising in Eq. (1) with identical oscillators and with regular coupling topology, where the contrast between system symmetry and observed coherence-incoherence patterns is more spectacular. However, the chimera phenomenon is usually robust with
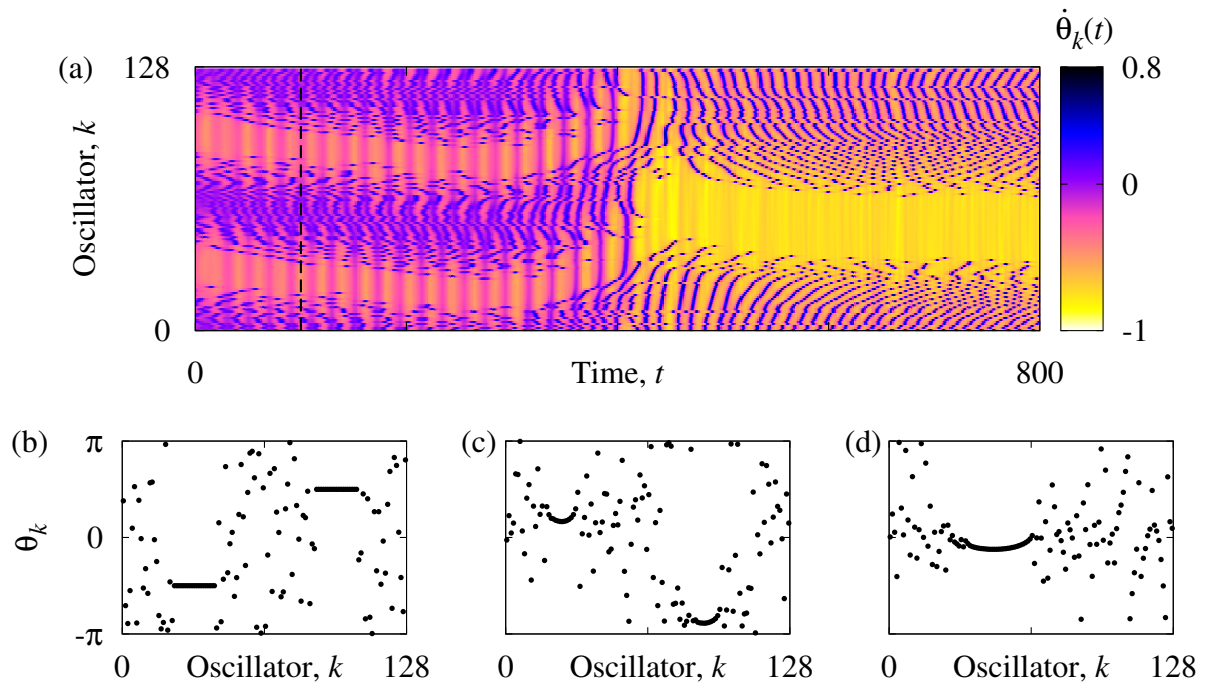
Figure 2: (a) Space-time plot of the phase velocities $\dot{\theta}_k(t)$ for the solution of Eq. (1) starting from the initial condition shown in panel (b). (c) Chimera state with two anti-phase coherent regions at $t = 100$ (vertical dashed line in (a)). (d) Chimera state with a single coherent region at $t = 800$. Parameters as in Fig. 1(c).

respect to perturbations of different types. For example, it persists if the natural frequencies of the oscillators are randomly chosen from a narrow width distribution [67], or if regular non-local coupling topology is slightly rewired [72, 177, 51].

Because of a special scaling in Eq. (1), coherence-incoherence patterns observed in this system for different sizes N have similar statistical properties, Fig. 3. This makes possible their analysis in the continuum limit $N \to \infty$. The advantage of such an approach (explained in detail in Section 3) comes from the fact that most of the dynamical regimes appearing as chaotic attractors or chaotic saddles in Eq. (1), correspond to fixed points and periodic orbits of the continuum limit equation. Note that
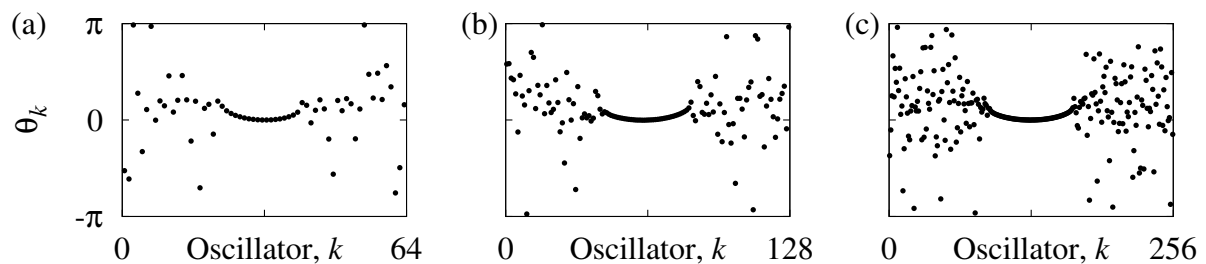
Figure 3: Snapshots of a chimera state in system (1) with (a) $N = 64$, (b) $N = 128$ and (c) $N = 256$ oscillators. Parameters are as in Fig. 1(c), except that $\alpha = \pi/2 - 0.15$.

q-twisted states and other coherent states are much simpler dynamical regimes than chimera states. They appear as periodic (or quasiperiodic) orbits already in the initial finite-N system (1), and they can be analyzed using the integral version of this model as explained in Remark 3.2.

Chimera states emerge not only in linear arrays but also in two- and higher-dimensional lattices. For example, by analogy with Eq. (1) one can write a two-dimensional model of non-locally coupled phase oscillators

$$\frac{d\theta_{jk}}{dt} = \omega_0 - \left(\frac{2\pi}{N}\right)^2 \sum_{n,m=1}^{N} G_2\left(\frac{2\pi}{N}(j-n), \frac{2\pi}{N}(k-m)\right)\sin(\theta_{jk}(t) - \theta_{nm}(t) + \alpha). \quad (5)$$

Here, $\{\theta_{jk}(t)\}_{j,k=1}^{N}$ are again the phases of the oscillators, ω_0 is their common natural frequency, $\alpha \in \mathbb{R}$ is the phase-lag parameter, and $G_2 : \mathbb{R}^2 \to \mathbb{R}$ is a non-constant coupling function, which is even and 2π-periodic with respect to both its arguments.
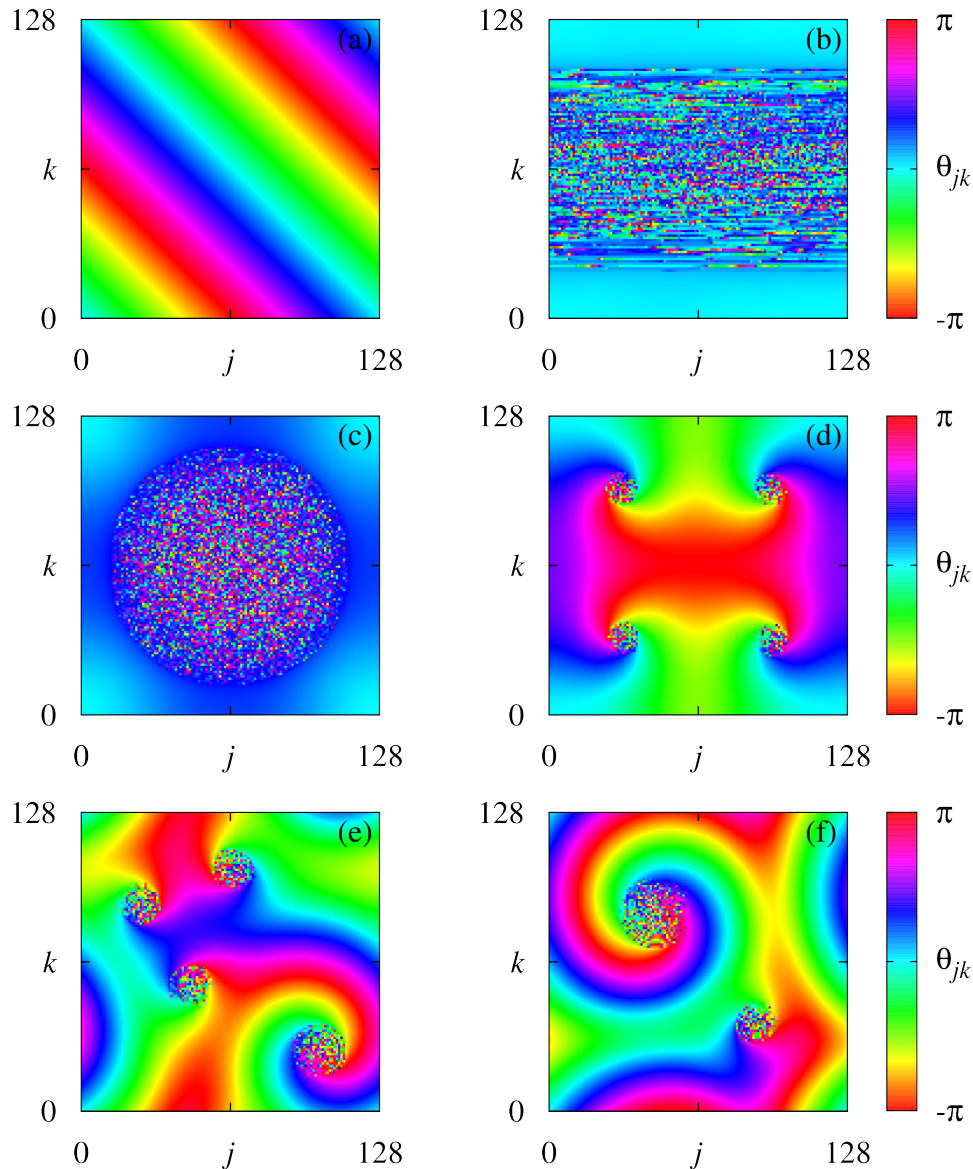
Figure 4: Solution snapshots in the $2D$-system (5) with the top-hat coupling (6). (a) $2D$-analog of the q-twisted states, (b)–(d) stationary chimera-like patterns, and (e)–(f) drifting chimera-like patterns. Parameters: $N = 128$, (a) $\sigma = 0.2$, $\alpha = 1.0$, (b) $\sigma = 0.8$, $\alpha = 1.44$, (c) $\sigma = 0.64$, $\alpha = 1.35$, (d) $\sigma = 0.2$, $\alpha = 0.6$, (e) $\sigma = 0.2$, $\alpha = 0.8$, (f) $\sigma = 0.2$, $\alpha = 0.9$.

Numerical simulations with a top-hat coupling function [58, 120]

$$G_2(x_1, x_2) = \begin{cases} (\pi\sigma^2)^{-1} & \text{for} \quad |x_1^2 + x_2^2| \leq \pi\sigma, \\ 0 & \text{for} \quad |x_1^2 + x_2^2| > \pi\sigma, \end{cases} \tag{6}$$

where $\sigma \in (0, 1)$ is the coupling radius, show chimera spots, chimera stripes and spiral chimeras existing for different parameter values, see Fig. 4. Similar patterns also exist in Eq. (5) with a trigonometric coupling [127, 175]

$$G_2(x_1, x_2) = \frac{1}{4\pi^2} \left(A_0 + A_1 \cos x_1 + A_1 \cos x_2 + A_2 \cos(2x_1) + A_2 \cos(2x_2) \right), \tag{7}$$

where $A_0, A_1, A_2 \in (0, \infty)$, as well as in Eq. (5) with other boundary conditions and other coupling functions [94, 38, 129, 82, 77].

Note that chimera spots and chimera stripes seem to be two-dimensional extensions of the corresponding one-dimensional patterns, whereas spiral chimeras are essentially two-dimensional patterns. This difference is also reflected in the fact that the former two patterns are observed for $\alpha \approx \pi/2$ as in Eq. (1), whereas stable spiral chimeras appear for 'unusual' parameters $\alpha \approx 0$.

The models (1) and (5) can be further generalized for three-dimensional lattices. In this case, appearance of chimera states becomes even more sophisticated [88, 90]. For example, the additional dimension makes possible the existence of linked and knotted chimera filaments [80] resembling analogous patterns in reaction-diffusion systems. In the opposite case, one can also think about the reduction of models (1) and (5) to a minimal ßerodimensional model with correspondingly simplified chimera states. Such models describing two coupled populations of globally coupled oscillators were suggested in [3] and are briefly described in Section 3, see Eqs. (22), (23).

3 Continuum limit approach to spatially extended oscillator systems

In this section we consider a general spatially extended oscillator system of size N defined in terms of the following ingredients.

(i) *Natural frequencies*: Let $\{\omega_k\}_{k=1}^N$ be a set of real numbers chosen randomly and independently from a distribution $h(\omega)$ such that

$$h(\omega) = \lim_{N \to \infty} \frac{1}{N} \sum_{k=1}^N \delta(\omega - \omega_k) \tag{8}$$

in the sense of measure convergence.

(ii) *Phase interaction*: Let $f : \mathbb{R} \to \mathbb{R}$ be a 2π-periodic function.

(iii) *Spatial topology*: Let $D \subset \mathbb{R}^M$ be a bounded domain with Lebesgue measure $|D|$ and $\{x_k\}_{k=1}^N$ be a set of points uniformly distributed in D such that

$$d(x) := \lim_{N \to \infty} \frac{1}{N} \sum_{k=1}^N \delta(x - x_k) = |D|^{-1} \tag{9}$$

in the sense of measure convergence. Moreover, let $g : D \times D \to \mathbb{R}$ be a given *coupling function*.

At this point we do not specify any smoothness requirements on the functions f and g, but we mention that in most of the applications these functions are either smooth, or at least piecewise-smooth. The only exception is the case of identical natural frequencies ω_k when the distribution $h(\omega)$ is a delta function. We also recall that distributions h and d are probability measures on $\mathbb{R}$ and D, respectively, and therefore satisfy the normalization condition

$$\int_{-\infty}^{\infty} h(\omega)d\omega = \int_D d(x)dx = 1. \tag{10}$$

Using the above notation we define an N-dimensional stochastic ODE system

$$\frac{d\theta_k}{dt} = \omega_k + \frac{1}{N}\sum_{j=1}^{N} g(x_k, x_j)f(\theta_j(t) - \theta_k(t)) + \xi_k(t), \quad k = 1, \ldots, N, \tag{11}$$

where $\xi_k(t)$ denotes an uncorrelated Gaussian noise with vanishing mean $\langle \xi_k(t) \rangle = 0$ and pairwise averages $\langle \xi_k(t)\xi_j(t') \rangle = 2\nu\delta_{kj}\delta(t-t')$ with $\nu \geq 0$. The prefactor $1/N$ is responsible for the mean field nature of the interaction between oscillators $\theta_k(t)$.

Obviously, Eq. (11) can be interpreted as a generalization of the models (1) and (5) from Section 1. Indeed, if in Eq. (11) we discard the noise term $\xi_k(t)$ and choose

$$\omega_k = \omega_0, \quad f(\theta) = \sin(\theta - \alpha), \quad x_k = -\pi + 2\pi k/N, \quad g(x, y) = 2\pi G_1(x - y),$$

then we obtain Eq. (1). This means that Eq. (1) is a particular realization of the system (11) with $\nu = 0$, $h(\omega) = \delta(\omega - \omega_0)$, $D = [-\pi, \pi]$ and $d(x) = 1/(2\pi)$. Similarly, one can demonstrate that model (5) is also a special case of Eq. (11).

For system (11) there exists a standard mean field reduction approach [27, Appendix B] asserting that in the continuum limit $N \to \infty$ the empirical measure

$$\rho_N(\theta, \omega, x, t) = \frac{1}{N}\sum_{k=1}^{N} \delta(\omega - \omega_k)\delta(x - x_k)\delta(\theta - \theta_k(t))$$

with a "typical" choice of natural frequencies ω_k and positions x_k converges almost surely to the solution $\rho(\theta, \omega, x, t)$ of the nonlinear Fokker-Planck equation

$$\frac{\partial \rho}{\partial t} + \frac{\partial}{\partial \theta}\left(\rho\left[\omega + \int_D dx' \int_{-\infty}^{\infty} d\omega' \int_0^{2\pi} g(x, x')f(\theta' - \theta)\rho(\theta', \omega', x', t)d\theta'\right]\right) = \nu\frac{\partial^2\rho}{\partial\theta^2} \tag{12}$$

with appropriate initial data. The derivation of Eq. (12) relies on a coupled hierarchy of equations analogous to the BBGKY hierarchy (Bogoliubov-Born-Green-Kirkwood-Yvon hierarchy) in the kinetic theory of gases, which one truncates formally by letting $N \to \infty$ and discarding all correlation terms. In some cases, Eq. (12) can be justified rigorously, for example, when the oscillators parameters (ω_k, x_k) and their initial values $\theta_k(0)$ are independent and identically distributed [17].

Note that Eq. (12) with $\nu = 0$ describes the dynamics of the deterministic system (11), without the noise terms $\xi_k(t)$. In this case, Eq. (12) is usually referred to as the *continuity equation*. In contrast to the Fokker-Planck equation, which is of parabolic type, the continuity equation is hyperbolic, and its solutions are therefore less regular. For example, they can be non-smooth and can contain discontinuities and singularities.

The usual way of constructing solutions to Eq. (12) is based on their representation as a Fourier series

$$\rho(\theta, \omega, x, t) = \frac{h(\omega)d(x)}{2\pi} \left(1 + \sum_{n=1}^{\infty} \left[\overline{u}_n(\omega, x, t)e^{in\theta} + u_n(\omega, x, t)e^{-in\theta} \right] \right), \tag{13}$$

where $u_n : \mathbb{R} \times D \times \mathbb{R} \to \mathbb{C}$ is the n-th Fourier coefficient, $\overline{u}_n$ denotes the complex conjugate of u_n, and where one factorizes explicitly the time-independent terms $h(\omega)$ and $d(x)$.

Inserting (13) into Eq. (12) and expanding the resulting equation in a Fourier series with respect to θ, one obtains an infinite chain of coupled integro-differential equations for the Fourier coefficients,

$$u_n(\omega, x, t) = \int_0^{2\pi} \frac{\rho(\theta, \omega, x, t)}{h(\omega)d(x)} e^{in\theta} d\theta,$$

which, by analogy with the globally coupled oscillator models [28], can be called the *local order parameters*. The word 'local' refers here to the fact that the order parameters $u_n(\omega, x, t)$ quantify correlation in the behaviour of oscillators with $\omega_k \approx \omega$ and $x_k \approx x$ only, and this property may vary depending on the choice of the argument (ω, x).

The infinite-dimensional system for $\{u_n\}$ is extremely complicated and so far has been considered in the case of global coupling [27, 28] or several globally coupled populations [71] only. However, in the noiseless case ($\nu = 0$) and for a specific choice of the phase interaction function f, its analysis can be significantly simplified via the invariant manifold reduction discovered by Ott and Antonsen in [124, 125]. Roughly speaking, their observation can be formulated as follows. In the noiseless case ($\nu = 0$) and for $f(\theta) = \sin(\theta - \alpha)$ almost all solutions ρ of Eq. (12) converge asymptotically in time to the invariant manifold defined in the next proposition.

Proposition 3.1 *Let*

$$f(\theta) = \sin(\theta - \alpha), \qquad \alpha \in \mathbb{R}.$$

Suppose that $u : \mathbb{R} \times D \times \mathbb{R} \to \mathbb{C}$ *is a solution to the equation*

$$\frac{du}{dt} = i\omega u(\omega, x, t) + \frac{1}{2}e^{-i\alpha}\mathcal{F}u - \frac{1}{2}e^{i\alpha}u^2(\omega, x, t)\mathcal{F}\overline{u}, \tag{14}$$

where

$$(\mathcal{F}u)(x, t) := \int_{-\infty}^{\infty} d\omega \int_D h(\omega)d(y)g(x, y)u(\omega, y, t)dy.$$

Moreover, suppose that $|u(\omega, x, t)| \le 1$.

Then, formula (13) with $u_n(\omega, x, t) = u^n(\omega, x, t)$ *yields a solution to equation (12) in the noiseless case* $\nu = 0$.

The benefits provided by Proposition 3.1 can be described as follows. If one is not interested in the transient dynamics of Eq. (12) and looks for established dynamical regimes only, then Eq. (12) can be replaced with Eq. (14). Although Eq. (14) is still an infinite-dimensional integro-differential equation, its phase space is spanned by the single local order parameter u instead of an infinite sequence $\{u_n\}$. Its analysis is therefore much simpler than the analysis of the initial equation (12). Moreover, Eq. (14) is usually able to reveal all chimera states, and coherent and partially coherent states observed in the discrete system (11) with the corresponding phase interaction function f.

Remark 3.1 *It is easy to verify, see [121, Lemma 2], that if $\mathcal{F}$ is a bounded operator on $L^\infty(\mathbb{R} \times D; \mathbb{C})$ then the set of admissible solutions*

$$U = \{u \in L^\infty(\mathbb{R} \times D; \mathbb{C}) \ : \ |u| \le 1\}$$

is flow-invariant with respect to Eq. (14). In other words, if at the instant $t = 0$ one has $u(\cdot, 0) \in U$ then $u(\cdot, t) \in U$ for all $t > 0$.

Moreover, for any solution $u(\cdot, t) \in L^\infty(\mathbb{R} \times D; \mathbb{C})$ to Eq. (14) its coherent region

$$S_{\mathrm{coh}}(u, t) = \{(\omega, x) \in \mathbb{R} \times D \ : \ |u(\omega, x, t)| = 1\}$$

and its incoherent region

$$S_{\mathrm{incoh}}(u, t) = \{(\omega, x) \in \mathbb{R} \times D \ : \ |u(\omega, x, t)| < 1\}$$

are also flow-invariant, i.e.

$$S_{\mathrm{coh}}(u, t) = S_{\mathrm{coh}}(u, 0) \quad \text{and} \quad S_{\mathrm{incoh}}(u, t) = S_{\mathrm{incoh}}(u, 0) \quad \text{for all} \quad t > 0.$$

Note that the above definition of coherent and incoherent regions agrees with the intuitive understanding of chimera states. Indeed, let us insert the coefficients $u_n(\omega, x, t) = u^n(\omega, x, t)$ into formula (13) and compute the probability density ρ and then the conditional probability density $\rho(\theta, \omega, x, t)/(h(\omega)d(x))$ at the point (ω, x). If $(\omega, x) \in S_{\mathrm{incoh}}(u, t)$ we obtain

$$\frac{\rho(\theta, \omega, x, t)}{h(\omega)d(x)} = P_u(\theta) := \frac{1}{2\pi} \frac{1 - |u|^2}{1 - 2|u|\cos(\theta - \arg u) + |u|^2}$$

i.e. a Poisson distribution (see Fig. 5). In particular, $\arg u$ gives the position of the distribution center, and $|u|$ characterizes the distribution width. For $(\omega, x) \in S_{\mathrm{coh}}(u, t)$ the distribution $P_u(\theta)$ degenerates into a delta function,

$$P_u(\theta) = \delta(\theta - \arg u).$$

On the other hand, for a large system (11) the probability $\rho(\theta, \omega, x, t)/(h(\omega)d(x))$ yields, by definition, the distribution of phases $\theta_k(t)$ for oscillators with $\omega_k \approx \omega$ and $x_k \approx x$. The delta distribution corresponds to phase-locked oscillators, and hence $|u(\omega, x, t)| = 1$ implies coherence, whereas drifting oscillators can be found only for distributions $P_u(\theta)$ with $|u| < 1$, so that $|u(\omega, x, t)| < 1$ implies incoherence.
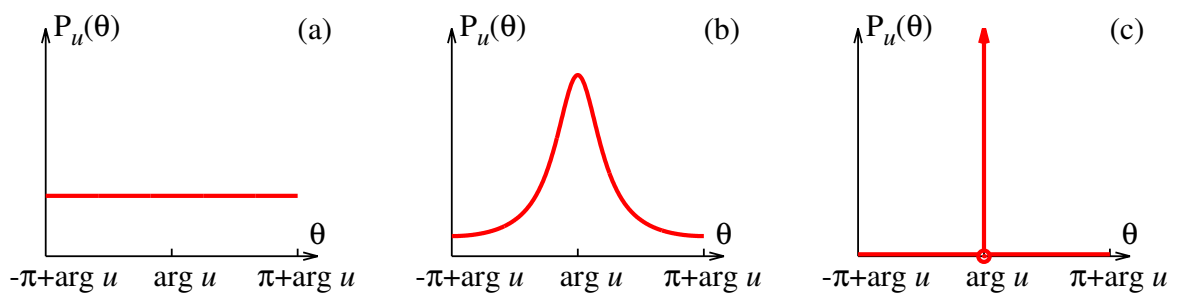

Figure 5: The Poisson distribution $P_u(\theta)$ for (a) $|u| = 0$, (b) $0 < |u| < 1$ and (c) $|u| = 1$.

Remark 3.2 *Let us consider Eq. (14) for identical oscillators with $h(\omega) = \delta(\omega)$. In this case the integration with respect to ω in expression $\mathcal{F}u$ becomes trivial and yields the integrand at $\omega = 0$. Therefore Eq. (14) can be restricted to the single point $\omega = 0$ and only $u(0, x, t)$ matters. The resulting reduced equation for $z(x, t) := u(0, x, t)$ reads*

$$\frac{dz}{dt} = \frac{1}{2}e^{-i\alpha}\mathcal{F}_0 z - \frac{1}{2}e^{i\alpha}z^2(x,t)\mathcal{F}_0\overline{z}, \tag{15}$$

where

$$(\mathcal{F}_0 z)(x, t) := \int_D d(y)g(x, y)z(y, t)dy. \tag{16}$$

Moreover, if a solution to Eq. (15) is everywhere coherent, i.e. $|z(x, t)| = 1$, then it can be rewritten in the form

$$z(x, t) = e^{i\Theta(x,t)} \quad \text{where} \quad \Theta : D \times \mathbb{R} \to \mathbb{R}.$$

Inserting this formula into Eq. (15) and performing straightforward transformations we find that in this case Eq. (15) is equivalent to the equation

$$\frac{\partial \Theta}{\partial t} = \int_D d(y)g(x, y)\sin(\Theta(y, t) - \Theta(x, t) - \alpha)dy, \tag{17}$$

which is an integral form of Eq. (11) for identical noiseless oscillators. Eq. (17) was used to study the existence and stability of q-twisted states [168, 102] and multi-twisted states [36] in a one-dimensional model (1) with a top-hat coupling function (3). It was also shown [98, 99, 100, 101] that Eq. (17) can appear as a graph limit for Kuramoto-like models on convergent sequences of random graphs.

Remark 3.3 *The oscillator positions x_k in the definition of the model (11) do not necessarily have to be uniformly distributed. Similar to the natural frequencies ω_k one can assume that the points x_k are chosen independently and randomly from a distribution $d(x)$ different from the uniform distribution but still satisfying the normalization condition (10). One can then again derive Eq. (12) and use the formula (13) to obtain Eq. (14) with the new function $d(x)$ appearing in the definition of the integral operator $\mathcal{F}$.*

To demonstrate the simplifying possibilities of the Ott-Antonsen reduction we now display several examples of Eq. (14) corresponding to different versions of the model (11) with $f(\theta) = \sin(\theta - \alpha)$.

Example 1. *Ott-Antonsen equation for model (1).*

For identical oscillators uniformly distributed in the interval $[-\pi, \pi]$ we take

$$h(\omega) = \delta(\omega), \quad D = [-\pi, \pi], \quad \text{and} \quad d(x) = \frac{1}{2\pi}.$$

Choosing $g(x, y) = 2\pi G_1(x - y)$, where $G_1(x)$ is the general even non-constant 2π-periodic function from the definition of model (1), and taking into account Proposition 3.1 and Remark 3.2 we find that the dynamics on the Ott-Antonsen manifold corresponding to the large-N system (1) is described by equation

$$\frac{dz}{dt} = \frac{1}{2}e^{-i\alpha}\mathcal{G}z - \frac{1}{2}e^{i\alpha}z^2(x,t)\mathcal{G}\overline{z}, \tag{18}$$

where

$$(\mathcal{G}v)(x) = \int_{-\pi}^{\pi} G_1(x - y)v(y)dy. \tag{19}$$

Given a solution $z(x,t)$ to Eq. (18) one can calculate the corresponding probability density $\rho(\theta, 0, x, t)$ using formula (13) with $u_n(0, x, t) = z^n(x, t)$.

Note that Eq. (1) corresponds to a special realization of the distribution $d(x)$, namely $x_k = -\pi + 2\pi k/N$ where $k = 1, \ldots, N$. It is not obvious that such realization is generic, although stable coherence-incoherence patterns predicted by Eq. (18) can usually be found [121, 174] in numerical simulations with the model (1).

Example 2. *Ott-Antonsen equation for a heterogeneous version of model (1).*

Let the oscillators be uniformly distributed in the interval $[-\pi, \pi]$ but have non-identical natural frequencies ω_k drawn from the Lorentzian distribution

$$h(\omega) = \frac{1}{\pi} \frac{\gamma}{\omega^2 + \gamma^2}.$$

Then, the domain D and the measure $d(x)$ remain the same as in Example 1, but now one cannot discard the ω-dependence of the local order parameter u. Nevertheless, there exists a special mathematical trick suggested in [124] and developed in [67, 70] that allows us to keep the resulting equation (14) as simple as Eq. (18).

Suppose that solution $u(\omega, x, t)$ to Eq. (14) has an analytic extension in the complex half-plane $\text{Im } \omega \geq 0$. Then applying residue theory one can compute

$$\int_{-\infty}^{\infty} h(\omega) u(\omega, x, t) d\omega = \int_{-\infty}^{\infty} \frac{\gamma}{\pi} \frac{u(\omega, x, t) d\omega}{\omega^2 + \gamma^2} = u(i\gamma, x, t).$$

Denoting $z(x, t) := u(i\gamma, x, t)$ and restricting Eq. (14) to the point $\omega = i\gamma$ we obtain a closed integro-differential equation

$$\frac{dz}{dt} = -\gamma z(x, t) + \frac{1}{2} e^{-i\alpha} \mathcal{G}z - \frac{1}{2} e^{i\alpha} z^2(x, t) \mathcal{G}\overline{z}, \tag{20}$$

where the integral operator $\mathcal{G}$ is the same as in formula (19). The additional term $-\gamma z$ in Eq. (20) plays a *dissipative* role, and solutions to Eq. (20) are therefore smoother than solutions to Eq. (18), see [67, 70].

Note that the relation between $z(x, t)$ and $\rho(\theta, \omega, x, t)$ is more involved in this case. To compute the probability density ρ one solves Eq. (14) with respect to u, assuming that

$$(\mathcal{F}u)(x, t) = (\mathcal{G}z)(x, t)$$

is already known. This yields the ω-dependent solution u. Then its integer powers u^n are inserted as Fourier coefficients u_n into the formula (13) which determines ρ.

Example 3. *Ott-Antonsen equation for model (5).*

The model (5) can be associated with a system of identical oscillators uniformly distributed in a two-dimensional domain $D = [-\pi, \pi]^2$. Thus

$$h(\omega) = \delta(\omega) \quad \text{and} \quad d(x) = \frac{1}{4\pi^2}.$$

Choosing $g(x, y) = 4\pi^2 G_2(x_1 - y_1, x_2 - y_2)$, where $G_2(x_1, x_2)$ is the general coupling function from the definition of model (5) we obtain an equation of the same form as Eq. (18) where $z : D \times \mathbb{R} \to \mathbb{C}$ and the integral operator $\mathcal{G}$ is given by

$$(\mathcal{G}v)(x) = \int_{-\pi}^{\pi} dy_2 \int_{-\pi}^{\pi} G_2(x_1 - y_1, x_2 - y_2) v(y_1, y_2) dy_1. \tag{21}$$

Note that looking for solutions to this equation one has to keep in mind the periodic boundary conditions hidden implicitly in the definition of coupling function $G_2(x_1, x_2)$.

Remark 3.4 *Examples 1–3 show that the domain D containing the points x_k appears in the Ott-Antonsen equation only in the argument of the local order parameter z and in the definition of the integral operator $\mathcal{G}$. Therefore Eq. (18) and Eq. (20) can also be used in the case of a three-dimensional domain D provided one introduces a suitable triple integration over D in the definition of $\mathcal{G}$.*

Note that in the case of a domain D which is a two- or higher-dimensional surface in an appropriate Euclidian space, the explicit form of the integral $\mathcal{G}$ will depend on the chosen surface parametrization. Examples of this kind can be found in [129, 77] where one considers Ott-Antonsen equations for a system of phase oscillators uniformly distributed on a unit two-dimensional sphere with identical [129] or Lorentzian [77] natural frequency distributions.

Example 4. *Ott-Antonsen equation for a two-population model.*

Originally, the Ott-Antonsen approach was suggested as a reduction technique for a system of globally coupled phase oscillators [124, 125]. In this case, dynamics on the Ott-Antonsen invariant manifold is described by a single complex ordinary differential equation rather than by the more complicated integro-differential equation (18). Similar reduction can also be performed for systems consisting of two or more populations of globally coupled oscillators. Then the resulting reduced equation can be formally interpreted as equation (18) with an appropriate point measure $d(x)$.

For example, let us consider a two-population system of the form

$$\frac{\theta_k^1}{dt} = \frac{\mu_1}{N}\sum_{j=1}^{N}\sin(\theta_j^1 - \theta_k^1 - \alpha) + \frac{\mu_2}{N}\sum_{j=1}^{N}\sin(\theta_j^2 - \theta_k^1 - \alpha), \tag{22}$$

$$\frac{\theta_k^2}{dt} = \frac{\mu_1}{N}\sum_{j=1}^{N}\sin(\theta_j^2 - \theta_k^2 - \alpha) + \frac{\mu_2}{N}\sum_{j=1}^{N}\sin(\theta_j^1 - \theta_k^2 - \alpha), \tag{23}$$

where $\mu_1 \in \mathbb{R}$ is the coupling strength inside of each population and $\mu_2 \in \mathbb{R}$ is the coupling strength between the populations. In [3, 4] it was shown that for appropriate choice of parameter μ_1 and μ_2 the system (22)–(23) provides one of the simplest examples of chimera states, i.e. a dynamical regime where one of the populations is synchronized while the other behaves asynchronously. Obviously, the system (22)–(23) can be interpreted as a particular case of Eq. (11), where $\nu = 0$ (noise is switched off), $f(\theta) = \sin(\theta - \alpha)$, $h(\omega) = \delta(\omega)$ (oscillators are identical) and $d(x)$ is a two-point measure,

$$d(x) = \frac{1}{2}\delta(x - x_1) + \frac{1}{2}\delta(x - x_2) \quad \text{for some} \quad x_1 \neq x_2.$$

Note that equal prefactors $1/2$ appear in $d(x)$ because of the equal size N of two populations in (22)–(23). Moreover, because the total system size of two populations equals $2N$, for coupling function g we assume $g(x_1, x_1) = g(x_2, x_2) = 2\mu_1$ and $g(x_1, x_2) = g(x_2, x_1) = 2\mu_2$.

Inserting the above ingredients into formulas (15) and (16) we obtain a reduced system on the Ott-Antonsen manifold

$$\frac{dz_1}{dt} = \frac{1}{2}e^{-i\alpha}(\mu_1 z_1 + \mu_2 z_2) - \frac{1}{2}e^{i\alpha}z_1^2(t)(\mu_1\overline{z}_1 + \mu_2\overline{z}_2), \tag{24}$$

$$\frac{dz_2}{dt} = \frac{1}{2}e^{-i\alpha}(\mu_2 z_1 + \mu_1 z_2) - \frac{1}{2}e^{i\alpha}z_2^2(t)(\mu_2\overline{z}_1 + \mu_1\overline{z}_2). \tag{25}$$

Here instead of the spatially dependent local order parameter $z(x, t)$ only its values $z_1(t) = z(x_1, t)$ and $z_2(t) = z(x_2, t)$ at the points x_1 and x_2 where distribution $d(x)$ is localized now appear.

The model (24)–(25) was used in [3, 4] to explain the bifurcation scenarios for chimera states observed in the finite-N system (22)–(23). Generalizations of this model for non-identical phase oscillators with Lorentzian distribution of natural frequencies and for a three population model were considered in [68, 71] and [92, 93], respectively. More detailed bibliography concerning the two-population model can be found in review papers [128, 143]. Here, we only note that Eqs. (22)–(23) served as a prototype model leading to first experimental realizations of chimera states in coupled chemical [108] and mechanical [95] oscillators.

Remark 3.5 *Example 4 is instructive because it reveals not only the advantages but also the limitations of the Ott-Antonsen approach. Since the two populations of the system (22)–(23) interact via global coupling only, one can use the beautiful mathematical theory developed by Watanabe and Strogatz in [164, 165] and show rigorously that this system has $2(N-2)$ constants of motion and that its phase space is foliated by invariant 4-dimensional tori. It turns out that many solutions of the finite-N system (22)–(23) do lie on the Ott-Antonsen manifold described by reduced system (24)–(25) but not all! Examples of such unexpected solutions, which lie outside of the Ott-Antonsen manifold, were reported by Pikovsky and Rosenblum in [132] and were called quasiperiodic chimera states.*

Note that the Watanabe-Strogatz theory provides an alternative way of deriving the Ott-Antonsen equation for identical noiseless phase oscillators. Approximating the coupling function g with a suitable piecewise-constant function on $D \times D$ one obtains a system of the form (11) but with hierarchical structure, i.e. an oscillator system which is a network of many interacting populations. Watanabe-Strogatz phase space decomposition can be applied to each of these populations [132]. Then, for a special choice of constants of motion one obtains a system of ODEs which is a discretized version of the Ott-Antonsen equation (18).

Example 5. *Ott-Antonsen equation for the Kuramoto-Sakaguchi model.*

Suppose that the coupling function g is constant and equals $K \in \mathbb{R}$. Then the system (11) degenerates into the classical Kuramoto model for globally coupled phase oscillators [156, 5, 133]. If the phase interaction between oscillators is purely sinusoidal $f(\theta) = \sin(\theta - \alpha)$ and noise is switched off ($\nu = 0$), then the corresponding Ott-Antonsen equation is obtained by inserting $g(x, y) = K$ and $d(x) = 1/|D|$ into Eq. (14). This yields

$$\frac{dz}{dt} = i\omega z(\omega, t) + \frac{K}{2} e^{-i\alpha} \mathcal{H} z - \frac{K}{2} e^{i\alpha} z^2(\omega, t) \mathcal{H} \overline{z}, \qquad (26)$$

where $z(\omega, t) = u(\omega, x, t)$ is independent of x, and

$$\mathcal{H} v := \int_{-\infty}^{\infty} h(\omega) v(\omega) d\omega \qquad (27)$$

is a complex-valued functional. Eq. (26) resembles very much Eq. (18) pointing out the similarity between the classical Kuramoto model and the spatially extended systems (1) and (5). On the other hand, there are several differences making the Ott-Antonsen equation (26) much simpler than its spatially extended counterpart (18). First, the integral operator $\mathcal{H}$ is a rank-1 operator whereas the operator $\mathcal{G}$ has, in general, an infinite-dimensional range. Second, for periodic coupling functions G_1 and G_2 the Ott-Antonsen equation (18) is invariant under some translational symmetry/symmetries (see Examples 1–3). These two features are responsible for the appearance of new types of solutions in Eq. (18), see Section 3.1, which makes the dynamics of Eq. (18) richer in comparison with Eq. (26).

Remark 3.6 *The continuum limit approach and Ott-Antonsen manifold reduction find application in a much wider class of models than those described by Eq. (11). For example, using this method one can analyze collective behaviour of large scale networks of coupled oscillators where the role of spatial coordinates x_k is played by randomly chosen coupling strengths [48] or by node degrees [154, 184]. Other examples will be mentioned in Section 8.*

3.1 Chimera states in Eq. (18)

Below, we outline a general bifurcation analysis scheme for Eq. (18) suggested in [121]. It can be used to study the existence and stability of chimera states in the large-N model (1) for any given coupling function G_1. The method relies on continuation of the solution branches bifurcating from the completely incoherent state $z(x, t) = 0$.

In the first step we consider linearization of Eq. (18) around $z(x, t) = 0$:

$$\frac{dv}{dt} = \frac{1}{2}e^{-i\alpha}\mathcal{G}v. \tag{28}$$

New solutions of Eq. (18) can bifurcate from the completely incoherent state only if the integral operator on the right-hand side of Eq. (28) has *critical spectrum* σ_{cr}, i.e. spectrum on the imaginary axis. Since every even absolutely integrable 2π-periodic function $G_1(x)$ can be represented as a Fourier series

$$G_1(x) = g_0 + \sum_{k=1}^{\infty} 2g_k \cos(kx), \tag{29}$$

where

$$g_k = \frac{1}{2\pi}\int_{-\pi}^{\pi} G_1(x)\cos(kx)dx,$$

it is easy to verify that the operator $\frac{1}{2}e^{-i\alpha}\mathcal{G}$ has non-zero critical spectrum $\sigma_{\mathrm{cr}} \subset i\mathbb{R}\backslash\{0\}$ for $\alpha = \pm\pi/2$ only. In this case

$$\sigma_{\mathrm{cr}} = \bigcup_{k=1}^{\infty}\{\pm i\pi g_k\},$$

and every eigenvalue $i\pi g_k$ or $-i\pi g_k$ has a pair of eigenfunctions $e^{\pm ikx}$.

Because of the cubic character of the nonlinearity in Eq. (18) some of the solutions bifurcating from zero at the bifurcation values $\pm i\pi g_k$ can be written explicitly. To find them we insert ansatz

$$z(x, t) = ae^{i(kx+\Omega t)}, \qquad a \in (0, \infty), \qquad \Omega \in \mathbb{R}, \qquad k \in \mathbb{Z}, \tag{30}$$

into Eq. (18). Taking into account $\mathcal{G}e^{ikx} = 2\pi g_k e^{ikx}$ and cancelling identical non-zero terms from both sides of the resulting equation we obtain

$$i\Omega = \pi g_k e^{-i\alpha} - \pi g_k a^2 e^{i\alpha}. \tag{31}$$

For every $k \in \mathbb{Z}$ and $g_k \neq 0$ equation (31) has two types of solutions:

(i) $\alpha = \pm\pi/2$, $a \in (0, \infty)$ and $\Omega = -\pi g_k(1 + a^2)\sin\alpha$,

(ii) $\alpha \in \mathbb{R}$, $a = 1$ and $\Omega = -2\pi g_k \sin\alpha$.

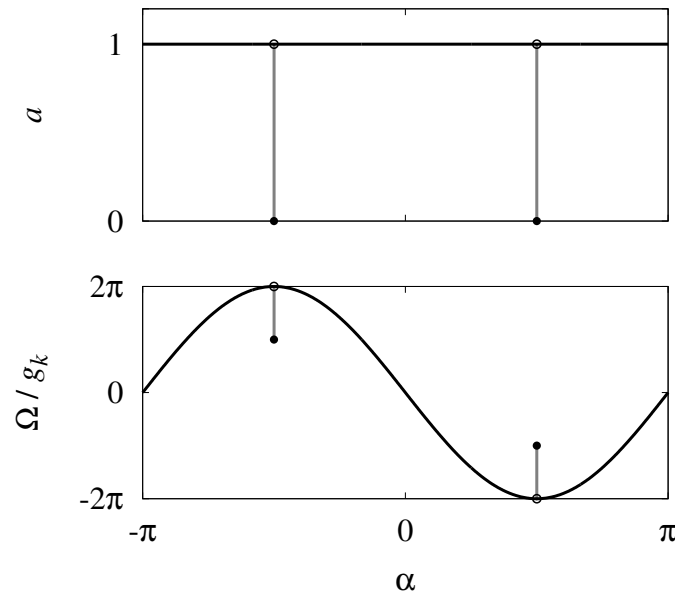Figure 6 shows these solutions without their problem irrelevant parts where $a > 1$ (recall that only

Figure 6: Parameters a and Ω of the solution to Eq. (18) given by formula (30) with $a \in [0, 1]$. Solution branch bifurcates from the completely incoherent state at the positions indicated with dots and has two qualitatively different parts: $a \in (0, 1)$ (gray) and $a = 1$ (black). Frequency Ω is normalized by the k-th Fourier coefficient g_k from formula (29).

functions $z(x, t)$ satisfying $|z| \leq 1$ can be interpreted as local order parameters). In accordance with the behaviour of the critical spectrum σ_{cr}, solution branches bifurcate from zero at points $(\alpha, a, \Omega) = (\pm\pi/2, 0, \mp\pi g_k)$ (dots in Fig. 6). At two other points $(\alpha, a, \Omega) = (\pm\pi/2, 1, \mp 2\pi g_k)$ (empty circles in Fig. 6) they undergo complex fold bifurcation, which as will be shown below also plays an important role in the emergence of chimera states.

Remark 3.7 *The complex fold bifurcation is a bifurcation with normal form [47]*

$$u^2 = p, \qquad u \in \mathbb{C}, \qquad p \in \mathbb{R},$$

see Fig. 7. In the vicinity of the points $(\alpha, a, \Omega) = (\pm\pi/2, 1, \mp 2\pi g_k)$, Eq. (31) can be transformed to this form using the non-degenerate coordinate transformation

$$u = \left(a e^{i\alpha} + \frac{i\Omega}{2\pi g_k a} \right) \left(1 \mp \frac{\Omega}{2\pi g_k a} \right)^{-1/2}, \qquad p = 1 \pm \frac{\Omega}{2\pi g_k a}.$$

Note that for $a = 1$ formula (30) yields the local order parameter of the q-twisted state with $q = k$, see Fig. 1(a). Moreover, in the case $k = 0$ this solution corresponds to the completely coherent state.

Due to its symmetries Eq. (18) has other solutions bifurcating from zero as well. Indeed, the equation is invariant under the following symmetry operations:

(i) complex phase shift: $z(x, t) \mapsto z(x, t)e^{i\varphi}$, where $\varphi \in \mathbb{R}$,

(ii) spatial translation: $z(x, t) \mapsto z(x + s, t)$, where $s \in \mathbb{R}$,

(iii) spatial reflection: $z(x, t) \mapsto z(-x, t)$.

Therefore it is natural to expect that it has *rotating wave* solutions of the form

$$z(x, t) = a(x)e^{i\Omega t}, \quad \text{where} \quad a \in C_{\mathrm{per}}([-\pi, \pi]; \mathbb{C}) \quad \text{and} \quad \Omega \in \mathbb{R}. \tag{32}$$
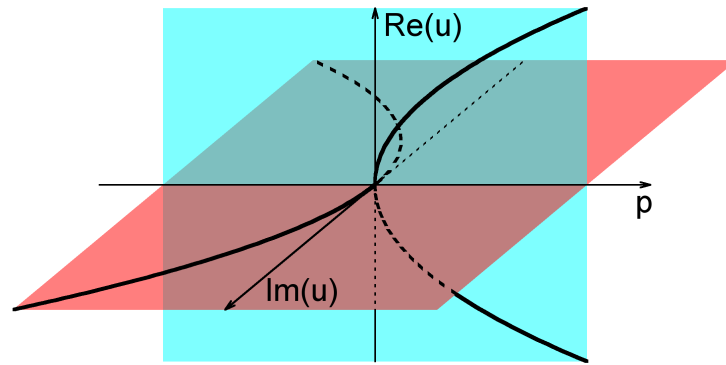
Figure 7: Complex fold bifurcation in the algebraic equation $u^2 = p$ with a complex unknown u and real parameter p.

Here and below we use the notation $C_{\mathrm{per}}([-\pi, \pi]; \mathbb{C})$ to denote the space of continuous periodic complex-valued functions on the interval $[-\pi, \pi]$.

Careful asymptotic analysis of Eq. (18) yields [121, Lemma 4]:

Proposition 3.2 *Suppose that g_k is a Fourier coefficient of the coupling function $G_1(x)$ such that $g_k \neq g_{(j+1)k}$ for all $j \in \mathbb{N}$. Then for $\alpha = \pi/2$ and for all sufficiently small $\varepsilon > 0$ there exists a solution to Eq. (18) of the following form*

$$z(x, t) = a_\varepsilon(x) e^{i\Omega_\varepsilon t}$$

where

$$a_\varepsilon(x) = \varepsilon \sin(kx) + O(\varepsilon^2), \quad \Omega_\varepsilon = -\pi g_k \left(1 + \frac{3}{4}\varepsilon^2 + O(\varepsilon^3)\right) \quad \text{for} \quad \varepsilon \to 0.$$

Moreover

$$a_\varepsilon(x) \in \mathrm{span}\left\{\sin(kx), \sin(2kx), \sin(3kx), \dots\right\}.$$

In contrast to the solutions of Eq. (18) defined by formula (30), solutions from Proposition 3.2 have a spatially modulated modulus $|a_\varepsilon(x)|$. However, these moduli are everywhere incoherent $|a_\varepsilon(x)| < 1$ and hence do not correspond to chimera states, which have to comprise both coherent and incoherent regions. In order to find chimera states one usually needs to extend these spatially modulated solutions far from zero, see example in Section 3.3.

A general computational scheme for the path-following of rotating waves (32) is described in [121, Section 3.2]. It relies on a scaled version of the self-consistency equation proposed by Kuramoto and Battogtokh [62]. More precisely, because of the cubic nonlinearity in Eq. (18), one can show that all stable rotating waves (32) satisfying the inequality $|z| \leq 1$ are given by the formula

$$z(x, t) = H(|w(x)|^2) w(x) e^{i\Omega t}, \tag{33}$$

where

$$H(s) := \begin{cases} \dfrac{1 - \sqrt{1-s}}{s} = \dfrac{1}{1 + \sqrt{1-s}} & \text{for} \quad 0 \le s < 1, \\[3mm] \dfrac{1 - i\sqrt{s-1}}{s} = \dfrac{1}{1 + i\sqrt{s-1}} & \text{for} \quad s \ge 1, \end{cases} \tag{34}$$

and where the triple $(\alpha, \Omega, w(x)) \in \mathbb{R}^2 \times C_{\text{per}}([-\pi, \pi]; \mathbb{C})$ satisfies a self-consistency equation of the form

$$\mu w(x) = \int_{-\pi}^{\pi} G_1(x - y) H(|w(y)|^2) w(y) dy \tag{35}$$

with the abbreviated complex parameter

$$\mu = i\Omega e^{i\alpha} = (-\Omega) e^{-i\beta} \quad \text{and} \quad \beta = \frac{\pi}{2} - \alpha. \tag{36}$$

Using standard solvers for integral equations one computes solution branches $(\mu, w(x)) \in \mathbb{C} \times C_{\text{per}}([-\pi, \pi]; \mathbb{C})$ of the nonlinear eigenvalue problem (35). These can then be transformed using formulas (33) and (36) into solutions of Eq. (18). The algorithm becomes especially simple for trigonometric coupling (4) when the integral equation (35) has finite rank and can be rewritten as a system of nonlinear algebraic equations.

It is important to emphasize that chimera states may appear not only on the primary branches of Eq. (18), which bifurcate from zero, but also on the secondary and higher order branches. For example, it is known [121, Lemma 5] that for $g_0 \ne 0$, a number of secondary branches can bifurcate from the solution (30) with $k = 0$ and $a \in (0, 1)$. Performing continuation of these branches one also can find chimera states.

Proposition 3.3 *Suppose that g_k is a Fourier coefficient of the coupling function $G_1(x)$ such that $g_k/g_0 \in (0, 1)$ and $g_k \ne g_{(j+1)k}$ for all $j \in \mathbb{N}$. Then for $\alpha = \pi/2$ and for all sufficiently small $\varepsilon > 0$ there exists a solution to Eq. (18) of the following form*

$$z(x, t) = a_\varepsilon(x) e^{i\Omega_\varepsilon t}$$

where

$$a_\varepsilon(x) = \frac{\sqrt{g_0^2 - g_k^2}}{|g_0| + |g_k|} + \varepsilon \cos(kx) + O(\varepsilon^2), \quad \Omega_\varepsilon = -\nu_k \left(1 + C_0 \varepsilon^2 + O(\varepsilon^3)\right) \quad \text{for} \quad \varepsilon \to 0,$$

and

$$\nu_k = 2\pi g_0^2 / (g_0 + g_k),$$

$$C_0 = \left(1 + \frac{2\pi g_k c_2 \sqrt{g_0^2 - g_k^2}}{|g_0|(\nu_k - 2\pi g_0 c_1)}\right)^{-1} \frac{\pi g_k}{4} \left(c_3 + \frac{4\pi g_0 c_2^2}{\nu_k - 2\pi g_0 c_1} + \frac{2\pi g_{2k} c_2^2}{\nu_k - 2\pi g_{2k} c_1}\right),$$

$$c_k = \frac{d^k}{du^k}\left(u H(u^2)\right)\bigg|_{u = \sqrt{1 - g_k^2/g_0^2}}, \quad k = 1, 2, 3.$$

Moreover

$$a_\varepsilon(x) \in \text{span} \left\{1, \cos(kx), \cos(2kx), \cos(3kx), \dots\right\}.$$

3.2 Stability of chimera states

Stability of rotating waves (33) can be analyzed by inserting the ansatz

$$z(x,t) = (a(x)e^{i\beta} + v(x,t))e^{i\Omega t}$$

into Eq. (18) and linearizing the resulting equation with respect to the small perturbation $v(x,t)$. This yields

$$\frac{dv}{dt} = -\Omega\eta\left(|w(x)|^2\right)v + \frac{1}{2}e^{-i\alpha}\left(\mathcal{G}v + a^2(x)\mathcal{G}\overline{v}\right),\qquad(37)$$

where

$$\eta(s) = -i(H(s)s - 1) = \begin{cases} i\sqrt{1-s} & \text{for} \quad 0 \le s < 1, \\ -\sqrt{s-1} & \text{for} \quad s \ge 1. \end{cases}\qquad(38)$$

The linear operator $\mathcal{L}$ appearing on the left-hand side of Eq. (37) is a sum of the multiplication operator $-\Omega\eta\left(|w(x)|^2\right)$ and a compact integral operator. In [121] it was shown that its spectrum $\sigma(\mathcal{L})$ consists of two parts, Fig. 8(a): essential spectrum $\sigma_{\text{ess}}(\mathcal{L})$ and point spectrum $\sigma_{\text{pt}}(\mathcal{L})$. The neutrally stable essential spectrum is known explicitly

$$\sigma_{\text{ess}}(\mathcal{L}) = \left\{-\Omega\eta\left(|w(x)|^2\right) \; : \; x \in [-\pi, \pi]\right\} \cup \{\text{c.c.}\} \subset \mathbb{R} \cup i\mathbb{R}.$$

The point spectrum $\sigma_{\text{pt}}(\mathcal{L})$ consists of a finite number of eigenvalues, which can be found by considering perturbations of the form

$$v(x,t) = v_+(x)e^{\lambda t} + \overline{v}_-(x)e^{\overline{\lambda}t}.\qquad(39)$$

In this case, formula (39) determines a solution to Eq. (37) provided λ and $(v_+, v_-)^{\text{T}}$ satisfy

$$\lambda\begin{pmatrix} v_+ \\ v_- \end{pmatrix} = \begin{pmatrix} -\Omega\eta(|w|^2)v_+ + \frac{1}{2}e^{-i\alpha}\left(\mathcal{G}v_+ + a^2\mathcal{G}v_-\right) \\ -\Omega\overline{\eta(|w|^2)}v_- + \frac{1}{2}e^{i\alpha}\left(\mathcal{G}v_- + \overline{a}^2\mathcal{G}v_+\right) \end{pmatrix},$$

or equivalently

$$\begin{pmatrix} v_+ \\ v_- \end{pmatrix} = \frac{1}{2}\begin{pmatrix} e^{-i\alpha}\left(\lambda + \Omega\eta(|w|^2)\right)^{-1}\left(\mathcal{G}v_+ + a^2\mathcal{G}v_-\right) \\ e^{i\alpha}\left(\lambda + \Omega\overline{\eta(|w|^2)}\right)^{-1}\left(\mathcal{G}v_- + \overline{a}^2\mathcal{G}v_+\right) \end{pmatrix}.\qquad(40)$$

Applying the integral operator $\mathcal{G}$ to both sides of Eq. (40) and denoting

$$V_+(x) = (\mathcal{G}v_+)(x), \quad V_-(x) = (\mathcal{G}v_-)(x),\qquad(41)$$

we obtain

$$\begin{pmatrix} V_+ \\ V_- \end{pmatrix} = \frac{1}{2}\begin{pmatrix} e^{-i\alpha}\mathcal{G}\left[(\lambda + \Omega\eta(|w|^2))^{-1}\left(V_+ + a^2V_-\right)\right] \\ e^{i\alpha}\mathcal{G}\left[\left(\lambda + \Omega\overline{\eta(|w|^2)}\right)^{-1}\left(V_- + \overline{a}^2V_+\right)\right] \end{pmatrix}.\qquad(42)$$

In general, Eq. (42) is difficult to analyze. However, for trigonometric coupling (4) and hence for a finite-rank integral operator $\mathcal{G}$ one can rewrite Eq. (42) as a finite-dimensional nonlinear eigenvalue problem and solve it numerically. The resulting eigenvalues are either real or appear as complex-conjugate pairs. They can be stable ($\text{Re }\lambda < 0$) or unstable ($\text{Re }\lambda > 0$). Thus one typically observes one of the following destabilization scenarios for chimera states: symmetry breaking, Fig. 8(b), Hopf bifurcation, Fig. 8(c), or non-standard Hopf bifurcation, Fig. 8(d). Note that in the first and the third bifurcation scenarios an unstable eigenvalue appears from the neutrally stable essential spectrum. This, in particular, explains why we call the bifurcation scenario in Fig. 8(d) the non-standard Hopf bifurcation.
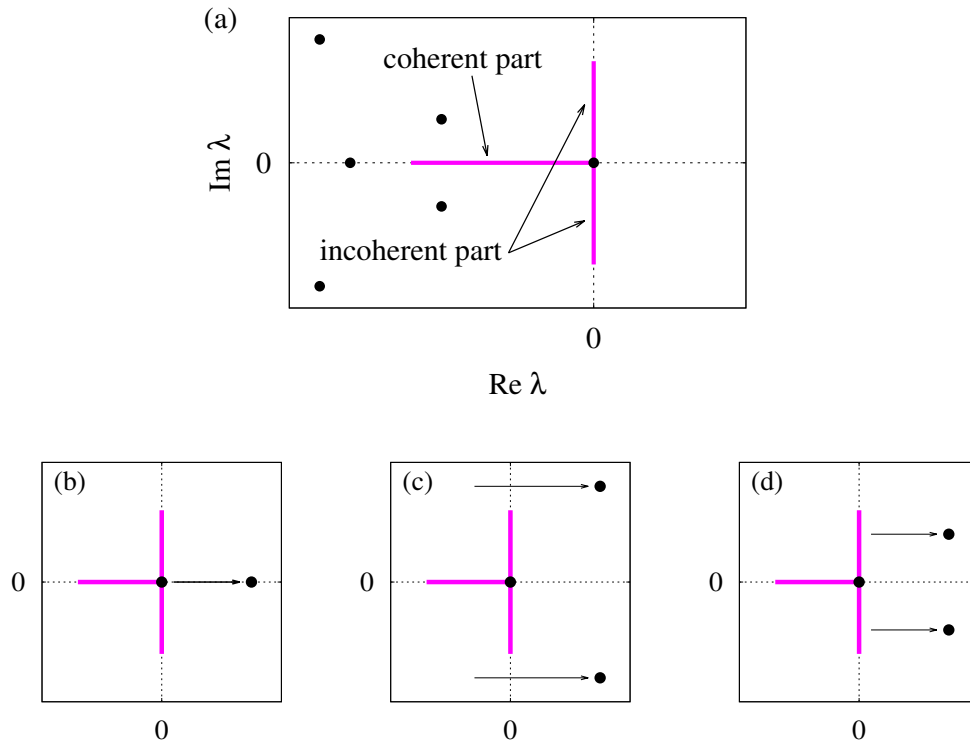
Figure 8: (a) Schematic structure of the spectrum $\sigma(\mathcal{L})$ corresponding to a stable chimera-like so-lution (32). The spectrum consists of an essential spectrum $\sigma_{\mathrm{ess}}(\mathcal{L})$ shown with the solid T-shaped curve and a finite number of eigenvalues (dots) constituting the point spectrum $\sigma_{\mathrm{pt}}(\mathcal{L})$. A zero eigen-value due to the continuous symmetries is embedded in the essential spectrum. Typical destabilization scenarios are symmetry breaking (b), Hopf bifurcation (c) and non-standard Hopf bifurcation (d).

3.3   Illustrative example

Let us consider a simple example illustrating the above bifurcation analysis scheme. We choose a trigonometric coupling function (4) with $A_0 = 1$, $A_1 \in (0, 2)$ and $A_2 = 0$. Then, formula (29) yields

$$g_0 = \frac{1}{2\pi}, \quad g_1 = \frac{A_1}{4\pi}, \quad \text{and} \quad g_k = 0 \quad \text{for all} \quad k \geq 2.$$

Formula (30) with $k = 0$, $a \in [0, 1]$, $\Omega = -\pi g_0 (1 + a^2)$ and Proposition 3.2 determine two solution branches of Eq. (18), which bifurcate from the completely incoherent state $z(x, t) = 0$. In Fig. 9 they are depicted as the two curves b_0 and b_1, respectively. Using Proposition 3.3 we also find the bifurcation point $\Omega = -\nu_1$ and a secondary solution branch b_2 bifurcating from the rotating wave (30) with $k = 0$. Spatial profiles of the rotating wave amplitudes $|a(x)|$ typical for branches b_0, b_1 and b_2 are shown in the panels adjacent to the main diagram of Fig. 9. Solving numerically the self-consistency equation (35) and substituting the result $(\mu, w(x))$ into formulas (33) and (36) allows us to extend the branches b_0, b_1 and b_2 until they reach complex fold bifurcations (empty circles). At these bifurcation points the profiles $|a(x)|$ touch for the first time the line $|a| = 1$, see panels b_0^c, b_1^c and b_2^c in Fig. 9. This tangency corresponds to the emergence of coherent regions.

An adequate representation of a complex fold requires a three-dimensional projection, see Fig. 7, therefore we continue with a three-dimensional diagram, Fig. 10, where along with the two coordi-nates Ω and $\|a\|$ we also use a third coordinate $\beta = \pi/2 - \alpha$. In Fig. 10 branches b_0, b_1 and b_2
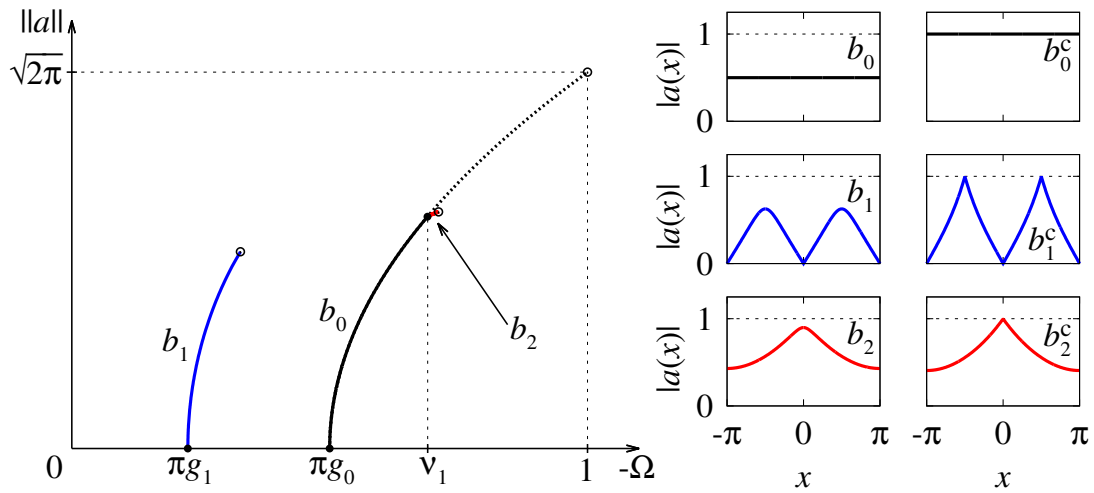
Figure 9: Bifurcation diagram of solutions to Eq. (18). Thick curves in the main panel show solutions (32) with $k = 0$ (branch b_0) and rotating waves of the form (32) (branches b_1 and b_2), using the collective frequency Ω and the L^2-norm $\|a\|$ of the amplitude $a(x)$ as coordinates. Solid and dashed curves denote stable and unstable branches. Adjacent panels b_0, b_1 and b_2 show profiles of the modulus $|a(x)|$ typical for each of these branches. The other three panels b_0^{c}, b_1^{c} and b_2^{c} show profiles $|a(x)|$ when the corresponding branch reaches a complex fold bifurcation (empty circles in the main diagram). Parameters: trigonometric coupling (4) with $A_0 = 1$, $A_1 = 0.9$ and $A_2 = 0$.

lie in the plane $\beta = 0$ and are shown as gray curves. Their extensions beyond the complex folds are three-dimensional curves with $\beta > 0$ denoted as B_0, B_1 and B_2, respectively. Typical profiles $|a(x)|$ corresponding to these branches are shown in the adjacent panels of Fig. 10. If we recall that conditions $|a(x)| = 1$ and $|a(x)| < 1$ are criteria for coherent and incoherent regions, then it is clear that branch B_0 represents a completely coherent state whereas branches B_1 and B_2 represent two different chimera states (compare with Fig. 11). Proceeding with the stability analysis as explained in Section 3.2, we find that branch B_0 never becomes unstable, whereas branches B_1 and B_2 lose their stability via a non-standard Hopf bifurcation, Fig. 8(d), and a fold bifurcation, respectively.

Remark 3.8 *Figure 7 suggests that at any complex fold point there should be four solution curves meeting together. Then, what about the complex folds in Fig. 10 where we find only two such curves? The answer is simple – two solution curves of Eq. (18) were discarded. One of them is irrelevant because it describes solutions which do not satisfy the inequality $|a(x)| \leq 1$, while the other discarded curve contains unstable solutions only.*

Similar argument [121, Section 2.3] is used to explain the choice of the branch of the square root in the definition of the function $H(s)$, e.g. formula (34). Therefore solving the self-consistency equation (35) we automatically obtain solution curves $b_0 - B_0$, $b_1 - B_1$ and $b_2 - B_2$ as continuous (but non-smooth) curves in a suitable phase space.

Now, one can easily imagine the bifurcation diagram corresponding to a general coupling function $G_1(x)$. In this case, formula (29) has infinitely many non-vanishing coefficients g_k, therefore Propositions 3.2 and 3.3 yield infinitely many branches bifurcating from the completely incoherent state $z(x, t) = 0$ and from the homogeneous solution (30) with $k = 0$. Extending these branches numerically one may expect to find arbitrarily many chimera states with different number of coherent and incoherent regions. This theoretical prediction agrees with the results of numerical studies reported in [183, 161, 87, 178].
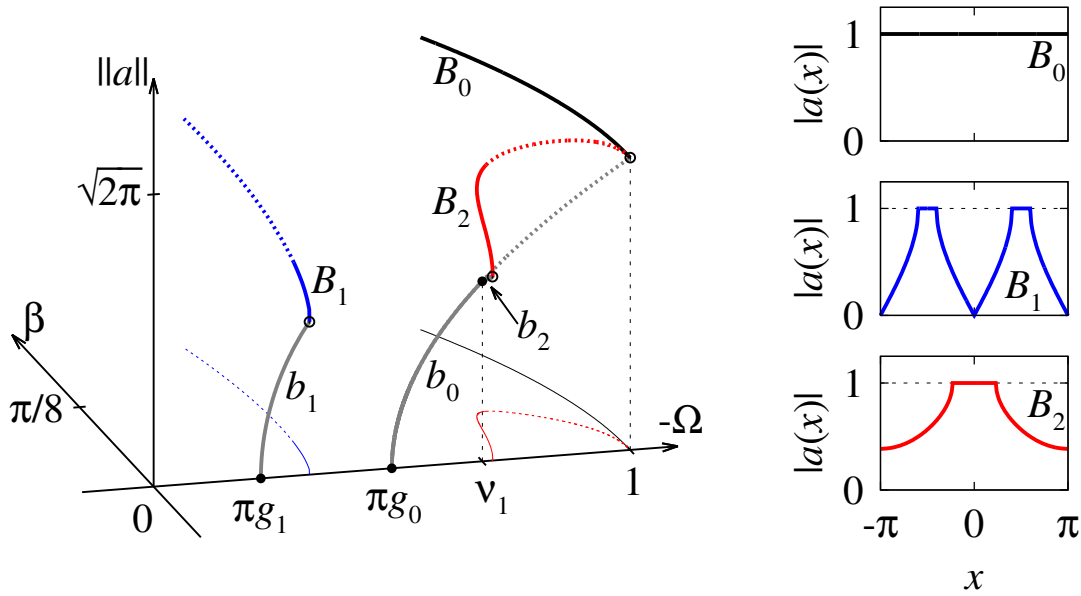
Figure 10: Extended bifurcation diagram of solutions to Eq. (18) with system parameter $\beta = \pi/2 - \alpha$ playing the role of the third coordinate. Branches B_0, B_1 and B_2 are extensions of the branches b_0, b_1 and b_2 from Fig. 9 beyond complex fold points (empty circles). Note that branches b_0, b_1 and b_2 lie in the plane $\beta = 0$. Thin curves are eye-guiding projections of the corresponding thick curves onto the plane (β, Ω). Adjacent panels show modulus profiles $|a(x)|$ typical for branches B_0, B_1 and B_2. Other parameters and notations are as in Fig. 9.

Remark 3.9 *If the coupling function $G_1(x)$ in (19) is the Green's function associated with the differential operator $-\partial_x^2 + 1$, then the integro-differential equation (18) can be rewritten as a system of two second-order ODEs. This transformation can be used to seek chimera states by means of phase plane analysis, or a shooting method and other techniques from the theory of finite-dimensional dynamical systems [70, 153].*

4   Finite size features of chimera states

The continuum limit equation (12) is a mean field equation valid for infinitely large systems (1) or (5). It cannot therefore explain all features of chimera states observed in finite-dimensional oscillator systems. For example, above we have seen that in the framework of the Ott-Antonsen equation (18) chimera states usually correspond to neutrally stable rotating waves (33). In contrast, their realizations in finite-N systems (1) have signs of extensive chaos [170, 19]. Fig. 12 shows Lyapunov spectra computed along chimera trajectories in the system (1) with the top-hat coupling (3). Each spectrum has a number of positive Lyapunov exponents, which is approximately proportional to the system size N. This observation agrees with the continuum limit conclusions, because for increasing system size the largest Lyapunov exponent tends to zero and hence chimera states can be identified as weakly chaotic attractors. The Lyapunov dimension N_L of this attractor is approximately proportional to the system size N and from the numerical simulations follows the existence of the limiting value

$$s_{\text{incoh}} = \lim_{N \to \infty} \frac{N_L}{N}$$

which coincides with the relative number of incoherent oscillators as $N \to \infty$. In fact, there are reasons to believe that as $N \to \infty$ the Lyapunov spectrum $\Lambda_N(s)$ converges to a curve representing
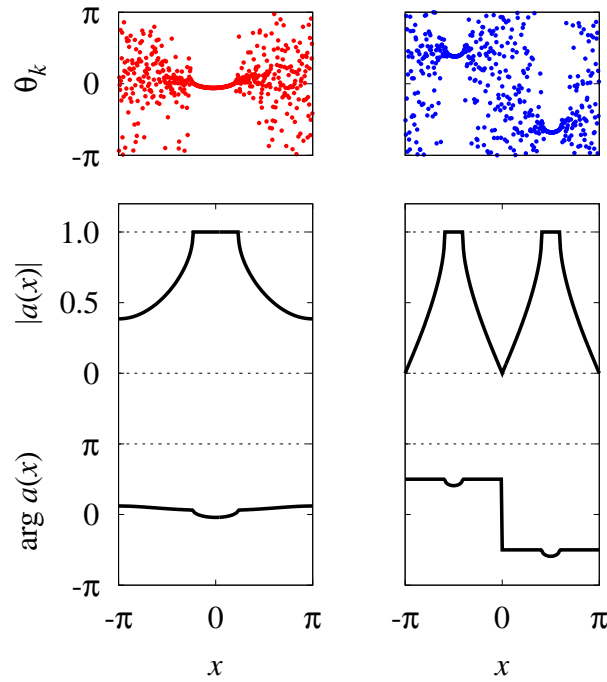
Figure 11: Chimera states in Eq. (1) and their representation as rotating wave solutions (32) in Eq. (18).

a suitably scaled spectral density of real parts $\mathrm{Re}\ \sigma(\mathcal{L})$, where $\sigma(\mathcal{L})$ is the spectrum of the linear operator $\mathcal{L}$ appearing in the linearization of Eq. (18) around the rotating wave corresponding to this chimera state.

Other features of chimera states going beyond their continuum limit description are irregular wandering of position [119] and a finite lifetime [171]. These properties play an important role if one considers chimera states of comparatively small size or monitors their behaviour on a large time-scale. Fig. 13 illustrates both phenomena in system (1) with $N = 40$ oscillators. Obviously, the macroscopic shapes of the coherent and incoherent regions do not vary in time, while the chimera state moves erratically as a rigid body. Extracting the trajectory of this motion and performing its statistical analysis we found [119] that it is described well by Brownian motion with a diffusion coefficient that scales inversely with some power of the system size N.

Fig. 13 also shows that small size chimera states usually collapse to the completely synchronized state[1]. The collapse time τ turns out to be extremely sensitive to initial data and behaves as a random variable[2] with an exponential distribution

$$E(\tau) = \frac{1}{T_\mathrm{m}} e^{-\tau/T_\mathrm{m}},$$

where T_m is the mean lifetime. Numerical simulations reveal exponential growth of T_m for increasing system size N such that

$$\log T_\mathrm{m} \sim N.$$

---

[1]Another type of collapse is shown in Fig. 2 where a chimera state with two coherent regions collapses to a chimera state with a single coherent region.

[2]Recent paper by Andrzejak et al. [6] reports that the sudden collapse of chimera states is promoted by a further decrease of synchronization, rather than by critically high synchronization. This fact can be used for short-term forecasting of collapse events.
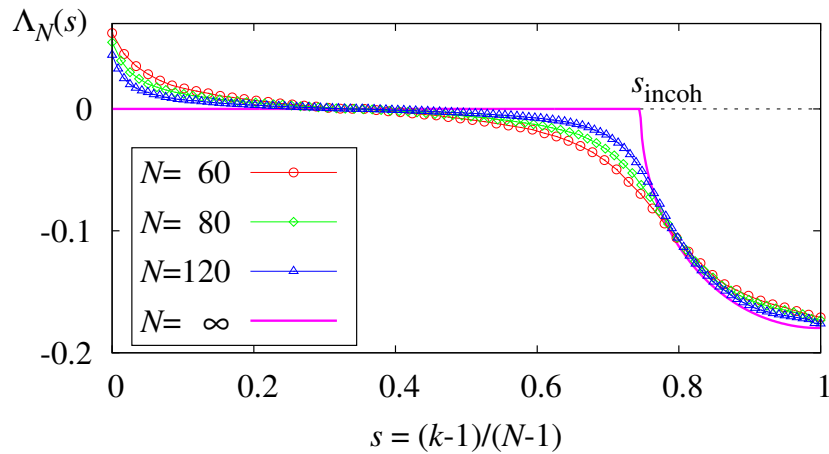
Figure 12: Lyapunov spectra $\Lambda_N(s)$ computed for chimera trajectories in the system (1) with the top-hat coupling (3) and different system sizes $N = 60$ (red circles), $N = 90$ (green diamonds), $N = 120$ (blue triangles). Parameters: $\sigma = 0.7$ and $\alpha = 1.5$.
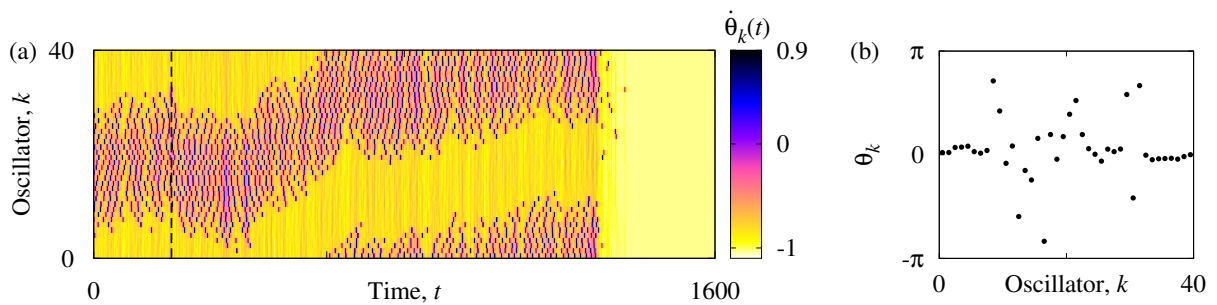

Figure 13: (a) Irregular position wandering and collapse of a chimera state in Eq. (1). (b) Snapshot of the chimera state at $t = 200$. Parameters: $N = 40$, $\alpha = 1.46$, top-hat coupling (3) with $\sigma = 0.7$.

Thus for system sizes $N > 60$ it is very unlikely that one observes even a single collapse event within the time span that is amenable to numerical simulation. Nevertheless it seems reasonable to identify most of the chimera states considered above as chaotic transients rather than as chaotic attractors.

Examples of chimera states which are true chaotic attractors can be obtained in modified versions of the system (1) when one applies some control (see Section 5) or when one uses a more complicated phase interaction function $f(\theta)$ (see [157]).

5 Control of chimera states

Propositions 3.2 and 3.3 indicate that for a general coupling function $G_1(x)$ equation (18) has countably many rotating wave solutions of the form (33). Extending numerically each of them we may expect to find chimera states for almost all phase lags α, see, for example, branch b_1 in Fig. 10. However, most of the chimera states found in such a way turn out to be unstable and therefore cannot be observed in the corresponding finite-N system (1). On the other hand, if the type of instability is known, then one can often suggest a suitable control technique that stabilizes this unstable solution. We illustrate this

approach with two examples.

5.1 Proportional control

Given a solution $z(x,t)$ to Eq. (18) let us define the quantity

$$r(t) = \frac{1}{2\pi}\left|\int_{-\pi}^{\pi} z(x,t)dx\right|, \tag{43}$$

which is a continuum limit analog of the Kuramoto global order parameter

$$R(t) = \frac{1}{N}\left|\sum_{k=1}^{N} e^{i\theta_k(t)}\right| \tag{44}$$

defined for system (1). Projecting the solution diagram from Fig. 10 onto the (α, r)-plane we obtain Fig. 14. Here, the completely incoherent state, e.g. $z(x,t) = 0$, and the completely coherent state, e.g. $z(x,t) = e^{i\Omega t}$ with $\Omega = -2\pi g_0 \sin\alpha$, correspond to the lines $r = 0$ and $r = 1$, respectively. Moreover, for every rotating wave (33) on the chimera branch B_2, the formula (43) yields a time-independent constant $r \in (0,1)$. Similarly, formula (43) transforms branch b_0 into a vertical segment $r \in [0,1]$ at $\alpha = \pi/2$.
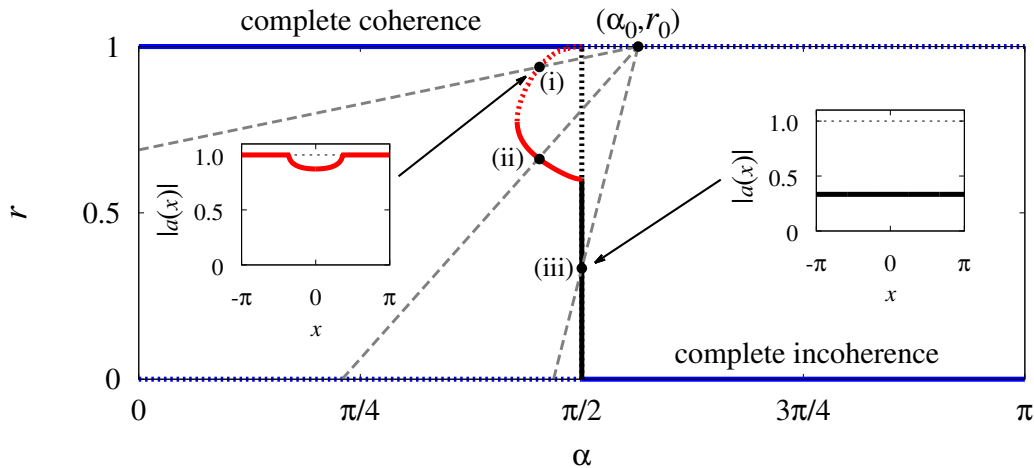
Figure 14: Projection of the solution diagram shown in Fig. 10 onto the (α, r)-plane. (i) Stabilization of an unstable chimera state. (ii) Collapse suppression. (iii) Stabilization of a uniformly drifting state.

In [152] it was shown that some unstable rotating wave solutions of Eq. (18) can be non-invasively stabilized using proportional control

$$\alpha = \alpha_0 + K(r - r_0), \qquad (\alpha_0, r_0) \in \mathbb{R}^2, \tag{45}$$

which makes the phase-lag parameter α and the measured order parameter r linearly dependent. Going back to the finite-N system (1) this control can be implemented by formula

$$\alpha = \alpha_0 + K(R - r_0). \tag{46}$$

However, in this case the control scheme (46) is non-invasive only on average, meaning that for a stabilized solution neither R nor α are constant, but oscillate irregularly around the values corresponding to a stabilized solution of Eq. (18).

Three examples of the application of proportional control are shown in Fig. 14, where dashed gray lines depict linear constraints (45) for three different values of the control gain K. Since the instability of the completely coherent state for $\alpha > \pi/2$ and of the completely incoherent state for $\alpha < \pi/2$ are both due to unstable essential spectra of the corresponding linearized operators, they persist in the controlled system (18), (45) as well. Therefore in Fig. 14 we choose the constraint lines (i)–(iii) starting from a pivot point (α_0, r_0) on the unstable part of the completely coherent state ($r = 1$) in order to guarantee the instability of this state. In order to analyze further the stabilizing role of proportional control one needs to look for intersections of the constraint line (45) with the projections of the branches b_0 and B_2 and then perform a linear stability analysis of found states with respect to the controlled system (18), (45), by analogy with Section 3.2.

(i) In this case proportional control stabilizes the chimera state on an unstable branch, which is inaccessible otherwise, see Fig. 15.
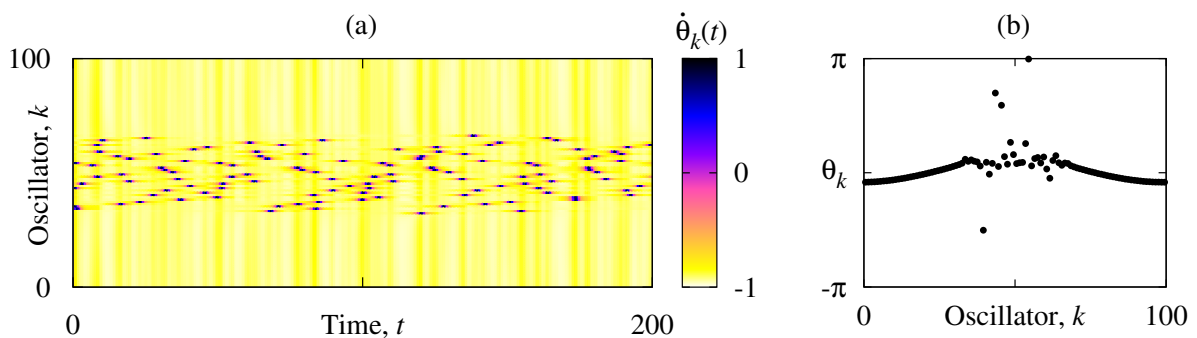

Figure 15: (a) Space-time plot and (b) snapshot of a chimera state in the system (1) stabilized using proportional control (46). Parameters: $N = 100$, trigonometric coupling (4) with $A_0 = 1$, $A_1 = 0.9$, and $A_2 = 0$. Control parameters: $\alpha_0 = \pi/2 + 0.2$, $r_0 = 1$, and $K = 5.7$.

(ii) In this case the constraint line (45) intersects a stable chimera branch but has no intersections with the stable part of the completely coherent state ($r = 1$), making chimera collapse impossible in this system. As a result, one can observe chimera states in the system (1) with relatively small sizes N. In some cases proportional control can also transform a chimera state into a global attractor, see Fig. 16.

(iii) In this case the constraint line (45) has a single intersection with the branch of uniformly drifting solutions. These solutions are difficult to observe in the original system, because they constitute a degenerate vertical branch for $\alpha = \pi/2$, see Fig. 17.

5.2   Position control

Another control scheme was suggested by Bick and Martens [12] to stabilize the position of a wandering chimera state. It relies on a feedback loop inducing a state-dependent asymmetry in the coupling function $G_1(x)$. More precisely, let us consider system (1) with a coupling function of the form

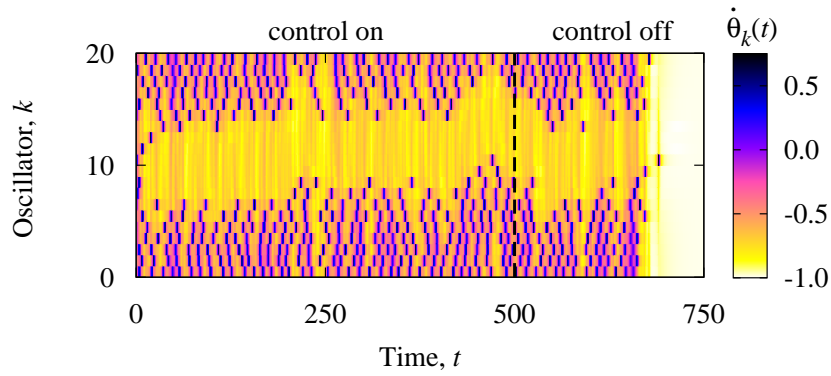$$G_1(x) = G_s(x) + \varepsilon G_a(x),$$

Figure 16: Proportional control (46) makes a chimera state into a global attractor of the system (1) so that it can be observed for small system sizes. After the control is switched off at $t = 500$ the chimera persists for some time before collapsing to the completely coherent state. Parameters: as in Fig. 15, except that $N = 20$ and $K = 1.05$.
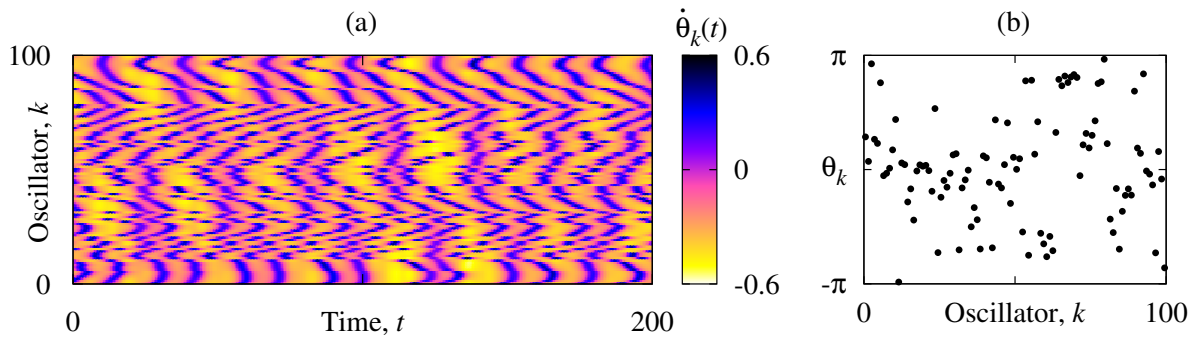
Figure 17: (a) Space-time plot and (b) snapshot of a uniformly drifting state ($r_{\mathrm{m}} = 1/3$) stabilized in the system (1) using proportional control (46). Parameters: as in Fig. 15, except that $N = 100$ and $K = 0.3$.

where $G_{\mathrm{s}}(x)$ and $G_{\mathrm{a}}(x)$ are even and odd functions, respectively. If for $\varepsilon = 0$ in the system (1) there exists a wandering chimera state with a single coherent region, then it can be pinned to a desired target position x_* by applying the control scheme

$$\varepsilon = \varepsilon_0 \Psi(\theta_1, \theta_2, \ldots, \theta_N; x_*),$$

where ε_0 is a sufficiently small number and Ψ is a function measuring the offset of the phase configuration $\{\theta_k\}$ with respect to the target x_*. By definition, function Ψ vanishes for zero offset, therefore obtained position control is non-invasive in the continuum limit $N \to \infty$ and non-invasive on average for finite-N system (1).

Both control schemes described above can be combined to suppress position wandering and collapse of the chimera simultaneously [116]. This allows one to observe chimera states in systems of small size, therefore resulting control scheme got the name *tweezer control*.

6 Chimera-like patterns in unbounded domains

Chimera-like patterns can be observed not only in bounded spatial domains, but also in infinite chains or lattices of coupled oscillators. A one-dimensional example of this kind was considered in [122, 173]. This is a chain of nonlocally coupled phase oscillators

$$\frac{d\theta_k}{dt} = \omega_k - \frac{K}{2P+1} \sum_{j=-P}^{P} \sin(\theta_k - \theta_{k+j} + \alpha), \quad k = \ldots, -1, 0, 1, \ldots, \tag{47}$$

whose natural frequencies are chosen from a unit-width Lorentzian distribution. If we assign uniformly distributed positions

$$x_k = \ell k = \frac{k}{2P}$$

to the oscillators and consider the formal limit $\ell \to 0$, requiring at the same time that ℓP remains constant, then for the probability density function $\rho(\theta, \omega, x, t)$ we obtain Eq. (12) on the real line $D = \mathbb{R}$ with the top-hat coupling function

$$G_1(x) = \begin{cases} K/2 & \text{for} \quad |x| \leq 1, \\ 0 & \text{for} \quad |x| > 1. \end{cases} \tag{48}$$

Using the Ott-Antonsen approach we reduce this equation to Eq. (20) with the coupling function (48) and $\gamma = 1$. The simplest solutions of the latter equation are the completely incoherent state $z(x,t) = 0$ and the plane waves

$$z(x,t) = ae^{i(\kappa x + \nu t)}, \qquad \kappa \in \mathbb{R},$$

corresponding to partially coherent twisted states. Stability analysis of these states reveals [122] that the interplay between the frequency inhomogeneity and nonlocal coupling results in the appearance of the well-known Eckhaus scenario, Fig. 18(a): A direct transition from stable incoherence to a stable
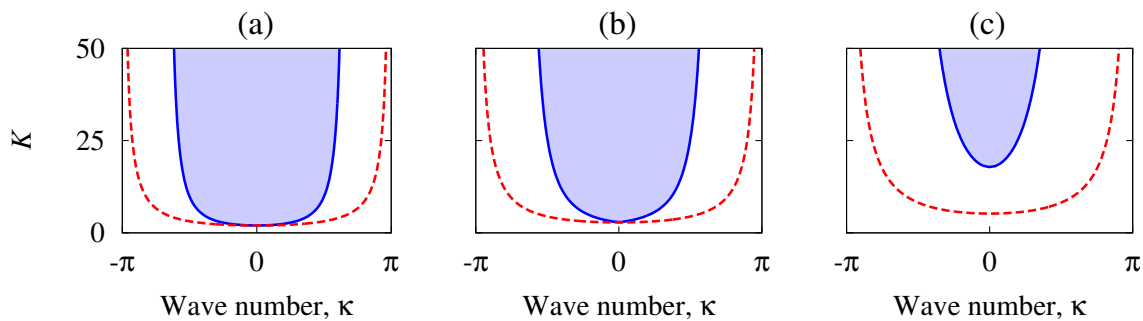
Figure 18: (Color online) Dashed curves show the existence boundaries for twisted states, which are also the instability boundaries for the uniformly incoherent state. Solid curves mark instabilities of twisted states. Stable twisted states can be found for parameters picked from the shaded regions. For increasing α, twisted states are less stable, compare (a) $\alpha = 0$, (b) $\alpha = \pi/4$, and (c) $\alpha = 3\pi/8$.

partially coherent state occurs only for the central wave number $\kappa = 0$. All other partially coherent twisted states with $\kappa \neq 0$ are unstable upon creation (dashed curve in Fig. 18(a)) and stabilize only for some $K > K_{\mathrm{E}}(\kappa)$ (shaded region in Fig. 18(a)).
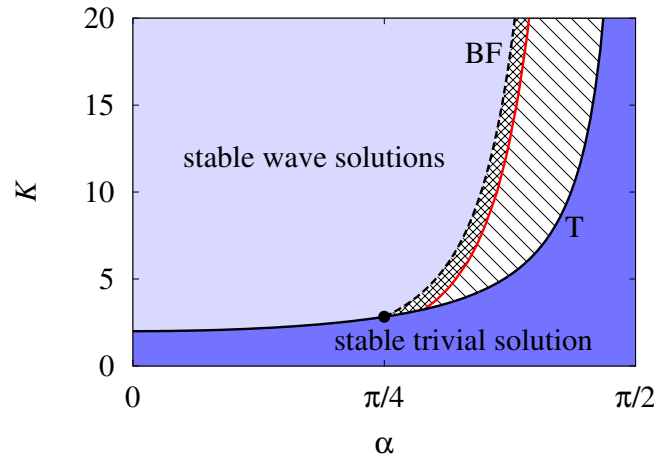
Figure 19: (Color online) Parameter regions where the trivial solution $z(x,t) = 0$ is stable (dark shaded) and Benjamin-Feir stable waves exist (light shaded). The region between the Benjamin-Feir instability (dashed line) and instability of the zero solution (solid line) corresponds to irregular dynamics and is divided into subregions of phase turbulence (shaded) and amplitude turbulence (hatched).

It turns out that for sufficiently large phase lag α and coupling strength K the completely incoherent state and the wave solutions are simultaneously unstable, see Fig. 18(c) and Fig. 19. For such parameters Eq. (20) exhibits spatiotemporal regimes of phase and amplitude turbulence [173], resembling to a certain extent the behaviour of chimera states.

Note that for the parameters close to the Benjamin-Feir instability one can use a perturbation analysis technique and derive the Kuramoto-Sivashinsky equation which provides an approximate description of the phase turbulence [56].

Remark 6.1 *If a spatially extended system of phase oscillators is coupled to another field variable with its own evolution equation, then the resulting system may become bistable [70]. This allows one to observe traveling synchronization fronts and localized bumps of synchrony, e.g. chimera solitons.*

7 Chimera states beyond phase oscillators

7.1 Chimera states in coupled limit cycle oscillators

The phase model (11) is relevant to a broad class of spatially extended oscillatory systems of the form [64]

$$\frac{\partial}{\partial t}A(x,t) = F(A(x,t)) + KS(x,t), \tag{49}$$

$$S(x,t) = \frac{1}{|D|}\int_D g(x,y)A(y,t)dy, \tag{50}$$

where $A \in \mathbb{R}^m$ is a vector state variable, $F : \mathbb{R}^m \to \mathbb{R}^m$ is a local nonlinearity, $K \in \mathbb{R}$ is a coupling strength, and $S \in \mathbb{R}^m$ is the mean-field coupling defined by (50). Assuming that the uncoupled system ($K = 0$) has an asymptotically stable limit cycle one can show [61] that for $K \approx 0$ and for a suitable

discretization of the integral (50), equation (11) describes phase reduced dynamics of the model (49)–(50). Accordingly, it is not a surprise that chimera states belong among the solutions of the model (49)–(50) at least in the weak coupling case. Indeed, already in their early work Kuramoto and colleagues reported chimera states in a complex Ginzburg-Landau equation with non-local coupling [62, 63] as well as in a system of non-locally coupled FitzHugh-Nagumo oscillators [63, 151]. Other examples of chimera states for a modified complex Ginzburg-Landau equation were found in [54] and [18].

In contrast to the phase oscillator, which is by definition one-dimensional, every limit cycle oscillator has two- or higher-dimensional local dynamics. Accordingly, the coupling between such oscillators may act via different local coordinates resulting in different local coupling schemes. For example, in the model (49)–(50) scalar coupling strength K can be replaced with a constant $m \times m$-matrix $\mathbf{K}$. Then the dynamics of the resulting system is determined not only by the local nonlinearity F and the coupling function g but also by the structure of the matrix $\mathbf{K}$. In particular, the choice of the matrix $\mathbf{K}$ can play a crucial role for the emergence of chimera states.

In [113] a model of non-locally coupled FitzHugh-Nagumo oscillators was considered. Performing its phase reduction and fitting the resulting system to equation (11) where $f(\theta) = \sin(\theta - \alpha)$ it was found that only an off-diagonal local coupling scheme $\mathbf{K}$ is capable of producing chimera states similar to those observed in Eq. (1). In contrast, with a diagonal matrix $\mathbf{K}$ one obtains coherent solutions only.

7.2   Beyond weak coupling

Above we discussed chimera states in the weak coupling limit only. But what happens when the coupling in Eq. (49) becomes stronger? This issue has been addressed in many special case studies relying on numerical simulations and statistical data analysis, see Appendix. Here, we mention only a few results summarized in the recent review [143].

Strong coupling usually suppresses oscillations, therefore for increasing coupling strength chimera states become more synchronized/coherent than their counterparts in the case of a weaker coupling. Since the interaction between oscillators is non-local, the oscillators do not synchronize homogeneously over the population, but exhibit a tendency to produce more complex coherence-incoherence patterns, where new coherent regions appear and grow inside of existing incoherent regions. The resulting patterns are usually called *many-cluster chimeras* or *multichimera states* [113]. In some cases these many-cluster chimeras start to travel [147]. Detailed parameter scans with respect to the coupling radius and coupling strength were computed for multi-cluster chimeras in coupled FitzHugh-Nagumo oscillators [113] and type-I excitable systems [163] as well as in coupled Hindmarsh-Rose [43] and Leaky integrate-and-fire neurons [160].

A qualitatively similar phenomenon called an *imperfect chimera state* was found in a system of coupled phase oscillators with inertia [50] and in the mathematical model describing the dynamics of coupled mechanical pendula [53]. In contrast to multichimera states, where the size of each coherent or incoherent region scales proportionally to the total number of oscillators N, in imperfect chimera state only a few distinct oscillators escape from the coherent region and rotate with an effective frequency different from other oscillators. In [53, 50] it was pointed out that dynamical mechanism responsible for the appearance of imperfect chimera states can be similar to that governing the appearance of solitary states in networks of globally coupled identical oscillators with attractive and repulsive interactions [86].

When the coupling between oscillators in the model (49)–(50) becomes too strong, oscillatory dynamics of the individual agents is completely suppressed and they settle at fixed points. Depending on the local coupling scheme $\mathbf{K}$ one can observe amplitude death or oscillation death. In the latter case a

variety of coexisting fixed point patterns, called *chimera death states* [181], can appear in the system. Their common feature is a patchy structure where in some regions oscillators are clustered together while in the other regions they are randomly distributed between several levels of different values.

7.3   Chimera states in locally coupled oscillators

Non-local coupling of the form (50) can naturally appear in certain reaction-diffusion systems. Suppose that the mean-field S evolves according to the equation

$$\tau \frac{\partial}{\partial t} S(x, t) = -S + \mu \Delta S + A(x, t), \tag{51}$$

where Δ is the Laplacian operator and $\mu > 0$ is a diffusion coefficient. If the time scale of Eq. (51) is much faster than the time scale of Eq. (49), e.g. $\tau \approx 0$, then setting $\tau = 0$ and solving Eq. (51) with respect to S one obtains formula (50), where $g(x, y)$ is the Green's function corresponding to the inverse operator $|D|(\mathrm{Id} - \mu \Delta)^{-1}$. In this case the reaction-diffusion system (49), (51) is likely to behave like the system (49)–(50). Note that instead of the discretizing equations (49)–(50) one can also discretize the pair of equations (49) and (51) keeping τ sufficiently small but non-vanishing. In this case, one obtains a system supporting chimera states where oscillators interact via purely *local* coupling [74].

Another dynamical mechanism leading to the emergence of chimera states in locally coupled oscillatory systems was described in [26]. It relies on the inherent bistability of the oscillators, when each of them can settle onto either a fixed point or a stable periodic orbit. Then weak local coupling supports formation of fronts connecting these two states, and if two fronts of opposite directions lock together, then they form a localized coherent/incoherent region of a chimera state.

7.4   Chimera states in globally coupled oscillators

Globally coupled identical phase oscillators always have identical effective frequencies [7], and cannot therefore support chimera states. However, this turns out to be false for globally coupled limit cycle oscillators whose state is described by a two- or higher-dimensional vector. In [148] it was shown that a relatively simple model

$$\frac{dW_k}{dt} = W_k - (1 + ic_2)|W_k|^2 W_k + K(1 + ic_1)\left(\frac{1}{N}\sum_{j=1}^{N} W_j - W_k\right) \tag{52}$$

consisting of N dynamical agents $W_k \in \mathbb{C}$ can develop, for a suitable choice of the real parameters c_1, c_2 and K, a chimera state where a fraction of the oscillators form a synchronized cluster and other oscillators drift with respect to the cluster and with respect to each other.

Later similar chimera states were found in a modified complex Ginzburg-Landau equation with a non-linear global coupling [140]

$$\frac{dW_k}{dt} = W_k - (1 + ic_2)|W_k|^2 W_k - \frac{1 + ic_1}{N}\sum_{j=1}^{N} W_j + \frac{1 + ic_2}{N}\sum_{j=1}^{N} |W_j|^2 W_j, \tag{53}$$

which is a simplified model describing electro-oxidation of silicon under illumination. In fact, interplay between linear and nonlinear global coupling gives rise to two types of chimera states with qualitatively different oscillator dynamics [141]. The phenomenon persists even when a linear diffusion term

is added on the right-hand side of Eq.(53). In particular, for a two-dimensional spatially extended version of Eq. (53) one observes bizarre chimera-like spatio-temporal patterns with stationary [141] and alternating [41] positions of the coherent and incoherent regions.

The dynamical mechanism leading to the emergence of chimera states in Eq. (52) and Eq. (53) is not yet satisfactorily clarified. In [142] it was pointed out that it is closely related to a clustering mechanism observed typically in globally coupled systems. Some progress in the analysis of the cluster break-up was done in [148, 60] based on the self-consistency approach. However, the true nature of the transition from clustered to chimera states still needs more detailed investigation.

7.5   Definition of chimera states

What is the definition of the chimera state? So far this question has no clear answer. As was pointed out in [107], the most striking features of chimera states are that they appear in coupled oscillator systems as a result of spontaneous symmetry breaking and that they usually coexist with a homogeneous, and therefore a more likely, synchronous state.

Already this loosely formulated description does not cover all the phenomena, which have been called 'chimeras' by different authors. For example, some of the 'chimeras' do not coexist with a homogeneous synchronous state [18]. Others were found for non-identical oscillators with Lorentzian distributed natural frequencies [67], i.e. in a non-symmetric system which is macroscopically homogeneous (coupling structure does not change from oscillator to oscillator) but locally heterogeneous (natural frequencies are randomly distributed). Even more questionable are chimera states in [117, 118], whose position in space is pre-determined by spatial profile of a delayed feedback signal. There are also 'chimeras' found in dynamical systems, which have no direct relation to coupled oscillators. These are spatially structured periodic orbits in coupled map lattices [112, 39] and arrays of locally coupled limit cycle oscillators [35] as well as special types of solutions in nonlinear delay differential equations motivated by laser dynamics, which look as chimera states in a virtual space-time representation and therefore are called *virtual chimera states* [78, 79, 144]. In view of this variety it remains rather unclear if there exists a general enough definition suitable for all the above phenomena. Here, we leave this question without an answer, but mention two promising attempts to do this.

A mathematically rigorous definition of a chimera state in coupled oscillator systems was suggested in [8, 13]. It is formulated in terms of the system symmetries and the symmetries of its solution. The definition, however, does not take into account such features of the chimera states as their position wandering [119] and spontaneous collapse to the completely synchronous state [171].

A phenomenological definition of chimera states suitable for coupled oscillator and other systems can be found in [57] where the authors defined two scalar quantities measuring spatial and time correlations of the coupled dynamical agents and used them to classify chimera states into stationary, turbulent and breathing chimeras.

8   Conclusion

In spite of numerous publications dealing with chimera states, there still remain a lot of unsolved problems in the field. Some of them are briefly outlined below.

It is very likely that the number of mathematical models supporting chimera states will continue to grow. In particular, using the Ott-Antonsen approach one can effectively study spatially extended mod-

els with neuroscience background, where phase oscillators are replaced with theta-neurons [84, 73] or where oscillators interact via a special form of coupling, called pulse coupling [126]. Even more complicated models can be constructed based on the derivation of firing-rate equations from a network of heterogeneous quadratic integrate-and-fire neurons, as suggested in [106, 75].

Another class of potentially interesting models are models with delays. At present, chimera states have been found in several spatially extended oscillatory systems with constant [67, 149, 85] and propagation [146] delays. More complicated models consisting of non-locally coupled phase oscillators with exponentially distributed delays in the interaction function were suggested and analyzed using the Ott-Antonsen approach in [81, 70]. For these models, a number of interesting spatiotemporal dynamical behaviours including fronts, spots, target patterns, chimeras, spiral waves and turbulent patterns were identified and described. We should also mention that models with constant delays play an important role in the mathematical description of chimeras observed in experiments with coupled chemical oscillators in [158, 159]. Finally, we note that chimera states can be expected in other models where delay appears not only in the coupling but also in the equation governing individual dynamics of the oscillators [180].

Apart from the spatially extended system (11) chimera states were also reported for more general random networks [72, 137, 184, 76, 51, 83], but corresponding studies were less systematic. For large size random networks properties of chimera states often can be explained using the continuum limit approach. On the other hand, for networks of moderate or small sizes it is more convenient to study them using the definition of 'weak' chimera state suggested in [8, 13]. This definition is based on the comparison of the network symmetry with the solution symmetry. It allows one to formulate and prove rigorously mathematical statements concerned with the properties of weak chimera states [8, 13, 14, 25]. Moreover, considering chimera states on small size networks one can obtain more detailed information about them applying standard bifurcation analysis tools for finite-dimensional dynamical systems [172, 130].

There still exists a number of interesting questions regarding 'classical' chimera states, e.g. chimeras in system (11). For example, in this model one assumes that the natural frequencies ω_k and oscillator positions x_k are uncorrelated. Moreover, the phase-lag parameter α appears there as a constant. On the other hand, already for the classical Kuramoto model it is known that inhomogeneous phase lags and their correlation with the natural frequencies can be responsible for significant changes in the bifurcation diagram changing a supercritical bifurcation into a subcritical one, for example, or resulting in the appearance of multistability [105]. Are similar phenomena possible in the model (11)? Partial answers to this question can be found in [97] (inhomogeneous phase lags) and in [176] (correlation between ω_k and x_k). However, a detailed study of this issue is still missing.

Little is known about the basin of attraction of chimera states. Its relative size has been estimated numerically in [152] and more detailed exploration was conducted in the case of a two-population model only [96].

As pointed out in Section 3, considering Eq. (12) one has an alternative: either to work with the infinite-dimensional dynamical system for the local order parameters $\{u_n\}$ or to apply the Ott-Antonsen manifold reduction. In the former case, one usually encounters serious technical problems as soon as the solution to Eq. (12) moves far from the completely incoherent state [27, 28, 103]. The problems are mainly due to the presence of a neutral essential spectrum in the spectrum of the corresponding linearized operator. This makes the constructions of classical bifurcation theory impossible. Some ways of overcoming this difficulty were proposed in recent papers concerned with the stability analysis of partially synchronized states in the classical Kuramoto model [23, 30]. However, the mathematical techniques employed there are so cumbersome that it is unclear if they can be easily transferred to

the chimera problem.

We should also mention another still unsolved mathematical problem concerned with the attractivity of the Ott-Antonsen manifold for non-locally coupled identical oscillators. More precisely, for globally coupled phase oscillators it is known [124, 125] that the Ott-Antonsen manifold is attracting for Lorentzian distributed natural frequencies but it loses this property in the case of identical oscillators. Were this so for non-locally coupled oscillators, it would contradict to the fact that Eq. (18) adequately describes stability properties of the chimera states in the discrete systems (1) and (5). One may argue that randomly distributed oscillator positions x_k play a dissipative role similar to that of distributed natural frequencies [131]. But, even if this were true, there appears the next question. The positions x_k in the models (1) and (5) are evenly distributed. Is this a 'typical' realization of the uniform distribution? The answer is not so obvious, especially if you take into account recent results about mode-locking in the classical Kuramoto model with evenly spaced natural frequencies [34].

Another interesting problem is to elaborate the continuum limit theory for a general phase interaction function $f(\theta)$ in Eq. (12) and for the noisy case with $\nu > 0$. As mentioned above, already a simple modification of the form

$$f(\theta) = \sin(\theta - \alpha) + \gamma \sin 2\theta, \quad \gamma > 0,$$

has a significant impact on the behaviour of chimera states [157]. On the other hand, the presence of noise in a non-locally coupled oscillator system can induce turbulence [55] or give rise to new types of chimera states [71, 145]. Moreover, beyond the continuum limit analysis there exists a challenging mathematical problem of explaining the finite size effects of chimera states (position wandering and collapse) and their scaling behaviour. Perhaps, these questions can be addressed using a finite size fluctuations theory, which can be developed by analogy with [42, 21, 22].

Chimera states were observed in computer-driven experiments with chemical oscillators [158, 108, 159], optical coupled map lattices [39] and networks of electronic logic circuits [136]. Later they were also found in experiments with coupled metronomes [95, 53, 32] and electrochemical oscillators [166, 167, 140]. However, it still remains unclear whether they can appear in natural systems beyond laboratory experiments. Their comparison with the *bump states* in neuroscience [65, 66], the unihemispherical sleep of animals [134] or with the *laminar-turbulent patterns* in a Couette flow [9] is rather speculative and requires more rigorous justification.

Hopefully some of the above problems will be elaborated on during the next decade contributing to improved understanding of the dynamical mechanisms governing the behaviour of chimera states. However, further developments of the continuum limit theory may require considerable time and effort.

Appendix: Limit cycle oscillator systems with chimera states

Oscillator type	Coupling type	References
Stuart-Landau oscillator	1D-ring with nonlocal coupling	[62, 181, 52]
	2D-lattice with periodic boundary conditions and nonlocal coupling	[63]
	two populations with global coupling	[69]

	population with linear (and nonlinear) global coupling [1]	[148, 141]
FitzHugh-Nagumo model in oscillatory regime	1D-ring with nonlocal coupling	[113, 114, 116, 49]
	1D-ring with fractal topology	[114]
	2D-lattice with free boundary or periodic boundary conditions and nonlocal coupling	[63, 139]
Hindmarsh-Rose model	1D-ring with nonlocal coupling	[43]
	several populations with global coupling	[45]
	two-layer network with instantaneous or time-delayed nonlocal coupling in one of the layers	[91]
SNIPER model for type-I excitable system	1D-ring with nonlocal coupling	[163]
Leaky integrate-and-fire neuron	two populations with global pulse-coupling	[110]
	1D-ring with nonlocal coupling	[160]
	network with fractal topology	[160]
	2D-lattice with periodic boundary conditions and nonlocal coupling	[139]
a Hodgkin-Huxley-type model of thermally sensitive neuron	two populations with time-delayed global coupling	[37]
	1D-ring with time-delayed nonlocal coupling	[37]
Van der Pol oscillator	1D-ring with instantaneous or time-delayed nonlocal coupling	[10, 115, 116]
	network with instantaneous and time-delayed fractal connectivities	[162, 138]

---

[0]In [141] it was shown that this type of chimera states also persists if one adds a diffusion-like (local) coupling to the system.

Van der Pol-Duffing oscillator with external periodic forcing	1D-ring with nonlocal coupling	[31]
Two-dimensional ODE model called lattice limit cycle model	networks with fragmented and hierarchical connectivieites	[44]
Three-variable ODE model of replicator-mutation dynamics	1D-ring with nonlocal coupling	[59]
Phase oscillator with inertia	two populations with global coupling	[20, 111]
	1D-ring with nonlocal coupling	[50]
	network of three nodes with global coupling	[89]
Two-dimensional ODE model for a Josephson junction with periodic forcing	1D-ring with local coupling	[46]
	population with global coupling	[104]
Two-variable ZBKE model for the Belousov-Zhabotinsky reaction	two populations with time-delayed global coupling	[158]
	1D-ring with time-delayed nonlocal coupling	[108, 109, 159]
Mechanical model of a metronome	two or three populations with global coupling	[95, 15]
	network of three nodes with global coupling	[169]
Semiconductor laser modeled by a Lang-Kobayashi-type ODE system	network of four nodes with time-delayed global coupling	[16, 135]
	1D-ring with local coupling	[150]

| Opto-electronic oscillator modeled by a two-dimensional ODE system with time-delayed feedback | network of four nodes with time-delayed global coupling | [40] |
| Spin-torque oscillator | population with global coupling | [182] |

References

[1] D. M. Abrams and S. H. Strogatz. Chimera states for coupled oscillators. *Phys. Rev. Lett.*, 93:174102, 2004.

[2] D. M. Abrams and S. H. Strogatz. Chimera states in a ring of nonlocally coupled oscillators. *Int. J. Bif. and Chaos*, 16:21–37, 2006.

[3] D. M. Abrams, R. Mirollo, S. H. Strogatz, and D. A. Wiley. Solvable model for chimera states of coupled oscillators. *Phys. Rev. Lett.*, 101:084103, 2008.

[4] D. M. Abrams, R. Mirollo, S. H. Strogatz, and D. A. Wiley. Erratum: Solvable model for chimera states of coupled oscillators [Phys. Rev. Lett. 101, 084103 (2008)]. *Phys. Rev. Lett.*, 101:129902, 2008.

[5] J. A. Acerbrón, L. L. Bonilla, C. J. Pérez-Vicente, F. Ritort, R. Spigler. The Kuramoto model: a simple paradigm for synchronization phenomena. *Rev. Modern Phys.*, 77:137–185, 2005.

[6] R. G. Andrzejak, C. Rummel, F. Mormann, and K. Schindler. All together now: Analogies between chimera state collapses and epileptic seizures. *Sci. Rep.*, 6:23000, 2016.

[7] P. Ashwin and J. W. Swift. The dynamics of n weakly coupled identical oscillators. *J. Nonlinear Sci.*, 2:69–108, 1992.

[8] P. Ashwin and O. Burylko. Weak chimeras in minimal networks of coupled phase oscillators. *Chaos*, 25:013106, 2015.

[9] D. Barkley and L. S. Tuckerman. Computational study of turbulent-laminar patterns in Couette flow. *Phys. Rev. Lett.*, 94:014502, 2005.

[10] V. M. Bastidas, I. Omelchenko, A. Zakharova, E. Schöll, and T. Brandes. Quantum signatures of chimera states. *Phys. Rev. E*, 92:062924, 2015.

[11] B. K. Bera, S. Majhi, D. Ghosh, and M. Perc. Chimera states: Effects of different coupling topologies. *Europhys. Letters*, 118:10001, 2017.

[12] C. Bick and E. A. Martens. Controlling chimeras. *New J. Phys.*, 17:033030, 2015

[13] C. Bick and P. Ashwin. Chaotic weak chimeras and their persistence in coupled populations of phase oscillators. *Nonlinearity*, 29:1468–1486, 2016.

[14] C. Bick. Isotropy of angular frequencies and weak chimeras with broken symmetry. *J. Nonlinear Sci.*, 27:605–626, 2017.

[15] K. Blaha, R. J. Burrus, J. L. Orozco-Mora, E. Ruiz-Beltrán, A. B. Siddique, V. D. Hatamipour, and F. Sorrentino. Symmetry effects on naturally arising chimera states in mechanical oscillator networks. *Chaos*, 26:116307 (2016).

[16] F. Böhm, A. Zakharova, E. Schöll, and K. Lüdge. Amplitude-phase coupling drives chimera states in globally coupled laser networks. *Phys. Rev. E*, 91:040901, 2015.

[17] L. L. Bonilla. Stable nonequilibrium probability densities and phase transitions for mean-field models in the thermodynamic limit. *J. Stat. Phys.*, 46:659–678, 1987.

[18] G. Bordyugov, A. Pikovsky, and M. Rosenblum. Self-emerging and turbulent chimeras in oscillator chains. *Phys. Rev. E*, 82:035205, 2010.

[19] A. E. Botha. Characteristic distribution of finitetime Lyapunov exponents for chimera states. *Sci. Report*, 6:29213, 2016.

[20] T. Bountis, V. G. Kanas, J. Hizanidis, and A. Bezerianos. Chimera states in a two-population network of coupled pendulum-like elements. *Eur. Phys. J. Special Topics*, 223:721–728, 2014.

[21] M. A. Buice and C. C. Chow. Correlations, fluctuations, and stability of a finite-size network of coupled oscillators. *Phys. Rev. E*, 76:031118, 2007.

[22] M. A. Buice and C. C. Chow. Dynamic finite size effects in spiking neural networks. *PLOS Comp. Biol.*, 9:e1002872, 2013.

[23] H. Chiba and I. Nishikawa. Center manifold reduction for large populations of globally coupled phase oscillators. *Chaos*, 21:043103, 2011.

[24] H. Chiba and G. S. Medvedev. The mean field analysis for the Kuramoto model on graphs I. The mean field equation and transition point formulas. arXiv:1612.06493.

[25] Y. S. Cho, T. Nishikawa, and A. E. Motter. Stable chimeras and independently synchronizable clusters. *Phys. Rev. Lett.*, 119:084101, 2017.

[26] M. G. Clerc, S. Coulibaly, M. A. Ferré, M. A. García-Ñustes, and R. G. Rojas. Chimera-type states induced by local coupling. *Phys. Rev. E*, 93:052204, 2016.

[27] J. D. Crawford and K. T. R. Davies Synchronization of globally coupled phase oscillators: singularities and scaling for general couplings. *Physica D*, 125:1–46, 1999.

[28] H. Daido. Onset of cooperative entrainment in limit-cycle oscillators with uniform all-to-all interactions: bifurcation of the order function. *Physica D*, 91:24–66, 1996.

[29] H. Dietert. Stability and bifurcation for the Kuramoto model. *J. Math. Pures Appl.*, 105:451–489, 2016.

[30] H. Dietert, B. Fernandez, and D. Gérard-Varet. Landau damping to partially locked states in the Kuramoto model. arXiv:1606.04470.

[31] D. Dudkowski, Y. L. Maistrenko, and T. Kapitaniak. Occurrence and stability of chimera states in coupled externally excited oscillators. *Chaos*, 26:116306, 2016.

[32] D. Dudkowski, J. Grabski, J. Wojewoda, P. Perlikowski, Y. Maistrenko, and T. Kapitaniak. Experimental multistable states for small network of coupled pendula. *Sci. Reports*, 6:29833, 2016.

[33] V. Dziubak, Y. Maistrenko, and E. Schöll. Coherent traveling waves in nonlocally coupled chaotic systems. *Phys. Rev. E*, 87:032907, 2013.

[34] S. Eydam and M. Wolfrum. Mode-locking in systems of globally coupled phase oscillators. WIAS Preprint No. 2418, doi: 10.20347/WIAS.PREPRINT.2418.

[35] L. V. Gambuzza, A. Buscarino, S. Chessari, L. Fortuna, and R. Meucci, and M. Frasca. Experimental investigation of chimera states with quiescent and synchronous domains in coupled electronic oscillators. *Phys. Rev. E*, 90:032905, 2014.

[36] T. Girnyk, M. Hasler, and Y. Maistrenko. Multistability of twisted states in non-locally coupled Kuramoto-type models. *Chaos*, 22:013114, 2012.

[37] T. A. Glaze, S. Lewis, and S. Bahar. Chimera states in a Hodgkin-Huxley model of thermally sensitive neurons. *Chaos*, 26:083119, 2016.

[38] C. Gu, G. St-Yves, and J. Davidsen. Spiral wave chimeras in complex oscillatory and chaotic systems. *Phys. Rev. Lett.*, 111:134101, 2013.

[39] A. M. Hagerstrom, T. E. Murphy, R. Roy, P. Hövel, I. Omelchenko, and E. Schöll. Experimental observation of chimeras in coupled-map lattices. *Nature Phys.*, 8:658–661, 2012.

[40] J. D. Hart, K. Bansal, T. E. Murphy, and R. Roy. Experimental observation of chimera and cluster states in a minimal globally coupled network. *Chaos*, 26:094801, 2016.

[41] S. W. Haugland, L. Schmidt, and K. Krischer. Self-organized alternating chimera states in oscillatory media. *Sci. Rep.*, 5:9883, 2015.

[42] E. J. Hildebrand, M. A. Buice, and C. C. Chow. Kinetic theory of coupled oscillators. *Phys. Rev. Lett.*, 98:054101, 2007.

[43] J. Hizanidis, V. Kanas, A. Bezerianos and T. Bountis. Chimera states in networks of nonlocally coupled Hindmarsh-Rose neuron models. *Int. J. Bif. and Chaos.*, 24:1450030, 2014.

[44] J. Hizanidis, E. Panagakou, I. Omelchenko, E. Schöll, P. Hövel, and A. Provata. Chimera states in population dynamics: Networks with fragmented and hierarchical connectivities. *Phys. Rev. E*, 92:012915, 2015.

[45] J. Hizanidis, N. E. Kouvaris, G. Zamora-López, A. Díaz-Guilera, and C. G. Antonopoulos. Chimera-like states in modular neural networks. *Sci. Reports*, 6:19845, 2016.

[46] J. Hizanidis, N. Lazarides, and G. P. Tsironis. Robust chimera states in SQUID metamaterials with local interactions. *Phys. Rev. E*, 94:032219, 2016.

[47] M. E. Henderson and H. B. Keller. Complex bifurcation from real paths. *SIAM J. Appl. Math.*, 50:460–482, 1990.

[48] D. Iatsenko,P. V. E. McClintock, and A. Stefanovska. *Nat. Communications*, 5:4118, 2014. Glassy states and super-relaxation in populations of coupled phase oscillators.

[49] T. Isele, J. Hizanidis, A. Provata, and P. Hövel. Controlling chimera states: The influence of excitable units. *Phys. Rev. E*, 93:022217, 2016.

[50] P. Jaros, Y. Maistrenko, and T. Kapitaniak. Chimera states on the route from coherence to rotating waves. *Phys. Rev. E*, 91:022907, 2015.

[51] X. Jiang and D. M. Abrams. Symmetry-broken states on networks of coupled oscillators. *Phys. Rev. E*, 93:052202, 2016.

[52] P. Kalle, J. Sawicki, A. Zakharova, and E. Schöll. Chimera states and the interplay between initial conditions and non-local coupling. *Chaos*, 27:033110, 2017.

[53] T. Kapitaniak, P. Kuzma, J. Wojewoda, K. Czolczynski, and Y. Maistrenko. Imperfect chimera states for coupled pendula. *Sci. Rep.*, 4:6379, 2014.

[54] Y. Kawamura. Chimera Ising walls in forced nonlocally coupled oscillators. *Phys. Rev. E*, 75:056204, 2007.

[55] Y. Kawamura, H. Nakao, and Y. Kuramoto. Noise-induced turbulence in nonlocally coupled oscillators. *Phys. Rev. E*, 75:036209, 2007.

[56] Y. Kawamura. From the Kuramoto-Sakaguchi model to the Kuramoto-Sivashinsky equation. *Phys. Rev. E*, 89:010901, 2014.

[57] F. P. Kemeth, S. W. Haugland, L. Schmidt, I. G. Kevrekidis, and K. Krischer. A classification scheme for chimera states. *Chaos*, 26:094814, 2016.

[58] P.-J. Kim, T.-W. Ko, H. Jeong, and H.-T. Moon. Pattern formation in a two-dimensional array of oscillators with phase-shifted coupling. *Phys. Rev. E,* 70:065201, 2004.

[59] N. E. Kouvaris, R. J. Requejo, J. Hizanidis, and A. Díaz-Guilera. Chimera states in a network-organized public goods game with destructive agents. *Chaos*, 26:123108, 2016.

[60] W. L. Ku, M. Girvan, and E. Ott. Dynamical transitions in large systems of mean field-coupled Landau-Stuart oscillators: Extensive chaos and cluster states. *Chaos*, 25:123122, 2015.

[61] Y. Kuramoto. *Chemical Oscillations, Waves, and Turbulence*. Springer, Berlin Heidelberg New York, 1984.

[62] Y. Kuramoto and D. Battogtokh. Coexistence of coherence and incoherence in nonlocally coupled phase oscillators. *Nonlinear Phenomena in Complex Systems*, 5:380–385, 2002.

[63] Y. Kuramoto and S. Shima, Rotating spirals without phase singularity in reaction-diffusion systems. *Prog. Theor. Phys. Suppl.*, 150:115, 2003.

[64] Y. Kuramoto, S. Shima, D. Battogtokh, and Y. Shiogai. Mean-field theory revives in self-oscillatory fields with non-local coupling. *Prog. Theor. Phys. Suppl.*, 161:127–143, 2006.

[65] C. R. Laing and C. C. Chow. Stationary bumps in networks of spiking neurons. *Neural Comput.*, 13:1473, 2001.

[66] C. R. Laing, W. C. Troy, B. Gutkin, and G. B. Ermentrout. Multiple bumps in a neuronal model of working memory. *SIAM J. Appl. Math.*, 63:62–97, 2002.

[67] C. R. Laing. The dynamics of chimera states in heterogeneous Kuramoto networks. *Physica D*, 238:1569–1588, 2009.

[68] C. R. Laing. Chimera states in heterogeneous networks. *Chaos*, 19:013113, 2009.

[69] C. R. Laing. Chimeras in networks of planar oscillators. *Phys. Rev. E*, 81:066221, 2010.

[70] C. R. Laing. Fronts and bumps in spatially extended Kuramoto networks. *Physica D*, 240:1960–1971, 2011.

[71] C. R. Laing. Disorder-induced dynamics in a pair of coupled heterogeneous phase oscillator networks. *Chaos*, 22:043104, 2012.

[72] C. R. Laing, K. Rajendran, and I. G. Kevrekidis. Chimeras in random non-complete networks of phase oscillators. *Chaos*, 22:013132, 2012.

[73] C. R. Laing. Derivation of a neural field model from a network of theta neurons. *Phys. Rev. E*, 90:010901, 2014.

[74] C. R. Laing. Chimeras in networks with purely local coupling. *Phys. Rev. E*, 92:050904, 2015.

[75] C. R. Laing. Exact neural fields incorporating gap junctions. *SIAM J. Appl. Dyn. Syst.*, 14:1899–1929, 2015.

[76] C. R. Laing. Bumps in small-world networks. *Front.Comput.Neurosci.*, 10:53, 2016.

[77] C. R. Laing. Chimeras in two-dimensional domains: heterogeneity and the continuum limit. *SIAM J. Appl. Dyn. Syst.*, 16:974–1014, 2017.

[78] L. Larger, B. Penkovsky, and Y. Maistrenko. Virtual chimera states for delayed-feedback systems. *Phys. Rev. Lett.*, 111:054103, 2013.

[79] L. Larger, B. Penkovsky, and Y. Maistrenko. Laser chimeras as a paradigm for multi-stable patterns in complex systems. *Nat. Communications*, 6:7752, 2015.

[80] H. W. Lau and J. Davidsen. Linked and knotted chimera filaments in oscillatory systems. *Phys. Rev. E*, 94:010204, 2016.

[81] W. S. Lee, J. G. Restrepo, E. Ott, and T. M. Antonsen. Dynamics and pattern formation in large systems of spatially-coupled oscillators with finite response times. *Chaos*, 21:023122, 2011.

[82] B.-W. Li and H. Dierckx. Spiral wave chimeras in locally coupled oscillator systems. *Phys. Rev. E*, 93:020202, 2016.

[83] B. Li and D. Saad. Chimera-like states in structured heterogeneous networks. *Chaos*, 27:043109, 2017.

[84] T. B. Luke, E. Barreto, and P. So. Complete classification of the macroscopic behavior of a heterogeneous network of theta neurons. *Neural Comput.*, 25:3207–3234, 2013.

[85] R. Ma, J. Wang, and Z. Liu. Robust features of chimera states and the implementation of alternating chimera states. *Europhys. Lett.*, 91:40006, 2010.

[86] Y. Maistrenko, B. Penkovsky, and M. Rosenblum. Solitary state at the edge of synchrony in ensembles with attractive and repulsive interactions. *Phys. Rev. E*, 89:060901, 2014.

[87] Y. Maistrenko, A. Vasylenko, O. Sudakov, R. Levchenko, and V. Maistrenko. Cascades of multi-headed chimera states for coupled phase oscillators. *Int. J. Bif. and Chaos.*, 24:1440014, 2014.

[88] Y. Maistrenko, O. Sudakov, O. Osiv, and V. Maistrenko. Chimera states in three dimensions. *New J. Phys.*, 17:073037, 2015.

[89] Y. Maistrenko, S. Brezetsky, P. Jaros, R. Levchenko, and T. Kapitaniak. Smallest chimera states. *Phys. Rev. E*, 95:010203, 2017.

[90] V. Maistrenko, O. Sudakov, O. Osiv, and Y. Maistrenko. Multiple scroll wave chimera states. *Eur. Phys. J. Special Topics*, 226:1867–1881, 2017.

[91] S. Majhi, M. Perc, and D. Ghosh. Chimera states in a multilayer network of coupled and uncoupled neurons. *Chaos*, 27:073109, 2017.

[92] E. A. Martens. Bistable chimera attractors on a triangular network of oscillator populations. *Phys. Rev. E*, 82:016216, 2010.

[93] E. A. Martens. Chimeras in a network of three oscillator populations with varying network topology. *Chaos*, 20:043122, 2010.

[94] E. A. Martens, C. R. Laing, and S. H. Strogatz. Solvable model of spiral wave chimeras. *Phys. Rev. Lett.*, 104:044101, 2010.

[95] E. A. Martens, S. Thutupalli, A. Fourrire, and O. Hallatschek. Chimera states in mechanical oscillator networks. *Proc. Natl Acad. Sci. USA*, 110:10563–10567, 2013.

[96] E. A. Martens, M. J. Panaggio, and D. M. Abrams. Basins of attraction for chimera states. *New J. Phys.*, 18:022002, 2016.

[97] E. A. Martens, C. Bick, and M. J. Panaggio. Chimera states in two populations with heterogeneous phase-lag. *Chaos*, 26:094819, 2016.

[98] G. S. Medvedev. Small-world networks of Kuramoto oscillators. *Physica D* 266:13–22, 2014.

[99] G. S. Medvedev. The nonlinear heat equation on W-random graphs. *Arch. Rational Mech. Anal.* 212:781–803, 2014.

[100] G. S. Medvedev. The nonlinear heat equation on dense graphs and graph limits. *SIAM J. Math. Anal.* 46:2743–2766, 2014.

[101] G. S. Medvedev and X. Tang. Stability of twisted states in the Kuramoto model on Cayley and random graphs. *J. Nonlinear Sci.*, 25:1169–1208, 2015.

[102] G. S. Medvedev and J. D. Wright. Stability of twisted states in the continuum Kuramto model. *SIAM J. Appl. Dyn. Syst.* 16:188–203, 2017.

[103] R. Mirollo and S. H. Strogatz. The spectrum of the partially locked state for the Kuramoto model. *J. Nonlinear Sci.*, 17:309–347, 2007.

[104] A. Mishra, S. Saha, P. K. Roy, T. Kapitaniak, and S. K. Dana. Multicluster oscillation death and chimeralike states in globally coupled Josephson Junctions. *Chaos*, 27:023110, 2017.

[105] E. Montbrió and D. Pazó. Shear diversity prevents collective synchronization. *Phys. Rev. Lett.*, 106:254101, 2011.

[106] E. Montbrió, D. Pazó, and A. Roxin. Macroscopic description for networks of spiking neurons. *Phys. Rev. X*, 5:021028, 2015.

[107] A. E. Motter. Spontaneous synchrony breaking. *Nature Phys.*, 6:164–165, 2010.

[108] S. Nkomo, M. R. Tinsley, and K. Showalter. Chimera states in populations of nonlocally coupled chemical oscillators. *Phys. Rev. Lett.*, 110:244102, 2013.

[109] S. Nkomo, M. R. Tinsley, and K. Showalter. Chimera and chimera-like states in populations of nonlocally coupled homogeneous and heterogeneous chemical oscillators. *Chaos*, 26:094826, 2016.

[110] S. Olmi, A. Politi, and A. Torcini. Collective chaos in pulse-coupled neural networks. Europhys. Lett., 92:60007, 2010.

[111] S. Olmi. Chimera states in coupled Kuramoto oscillators with inertia. *Chaos*, 25:123125, 2015.

[112] I. Omelchenko, Y. Maistrenko, P. Hövel, and E. Schöll. Loss of coherence in dynamical networks: spatial chaos and chimera states. *Phys. Rev. Lett.*, 106:234102, 2011.

[113] I. Omelchenko, O. E. Omel'chenko, P. Hövel, and E. Schöll. When nonlocal coupling between oscillators becomes stronger: patched synchrony or multichimera states. *Phys. Rev. Lett.*, 110:224101, 2013.

[114] I. Omelchenko, A. Provata, J. Hizanidis, E. Schöll, and P. Hövel. Robustness of chimera states for coupled FitzHugh-Nagumo oscillators. *Phys. Rev. E*, 91:022917, 2015.

[115] I. Omelchenko, A. Zakharova, P. Hövel, J. Siebert, and E. Schöll. Nonlinearity of local dynamics promotes multi-chimeras. *Chaos*, 25:083104, 2015.

[116] I. Omelchenko, O. E. Omel'chenko, A. Zakharova, M. Wolfrum, and E. Schöll. Tweezers for chimeras in small networks. *Phys. Rev. Lett.*, 116:114101, 2016.

[117] O. E. Omel'chenko, Y. L. Maistrenko, and P. A. Tass. Chimera states: The natural link between coherence and incoherence. *Phys. Rev. Lett.*, 100:044105, 2008.

[118] O. E. Omel'chenko, Y. L. Maistrenko, and P. A. Tass. Chimera states induced by spatially modulated delayed feedback. *Phys. Rev. E*, 82:066201, 2010.

[119] O. E. Omel'chenko, M. Wolfrum, and Y. L. Maistrenko. Chimera states as chaotic spatiotemporal patterns. *Phys. Rev. E*, 81:065201, 2010.

[120] O. E. Omel'chenko, M. Wolfrum, S. Yanchuk, Y. L. Maistrenko, and O. Sudakov. Stationary patterns of coherence and incoherence in two-dimensional arrays of non-locally coupled phase oscillators. *Phys. Rev. E*, 85:036210, 2012.

[121] O. E. Omel'chenko. Coherence-incoherence patterns in a ring of non-locally coupled phase oscillators. *Nonlinearity*, 26:2469–2498, 2013.

[122] O. E. Omel'chenko, M. Wolfrum, and C. R. Laing. Partially coherent twisted states in arrays of coupled phase oscillators. *Chaos*, 24:023102, 2014.

[123] O. E. Omel'chenko, M. Wolfrum, and E. Knobloch. Stability of spiral chimera states on a torus. WIAS Preprint No. 2417, doi: 10.20347/WIAS.PREPRINT.2417.

[124] E. Ott and T. M. Antonsen, Low dimensional behavior of large systems of globally coupled oscillators. *Chaos*, 18:037113, 2008.

[125] E. Ott and T. M. Antonsen. Long time evolution of phase oscillator systems. *Chaos*, 19:023117, 2009.

[126] D. Pazó and E. Montbrió. Low-dimensional dynamics of populations of pulse-coupled oscillators. *Phys. Rev. X*, 4:011009, 2014.

[127] M. J. Panaggio and D. M. Abrams. Chimera states on a flat torus. *Phys. Rev. Lett.*, 110:094102, 2013.

[128] M. J. Panaggio and D. M. Abrams. Chimera states: coexistence of coherence and incoherence in networks of coupled oscillators. *Nonlinearity*, 28:R67–R87, 2015.

[129] M. J. Panaggio and D. M. Abrams. Chimera states on the surface of a sphere. *Phys. Rev. E*, 91:022909, 2015.

[130] M. Panaggio, D. M. Abrams, P. Ashwin, and C. R. Laing. Chimera states in networks of phase oscillators: the case of two small populations. *Phys. Rev. E*, 93:012218, 2016.

[131] B. Pietras and A. Daffertshofer. Ott-Antonsen attractiveness for parameter-dependent oscillatory systems. *Chaos*, 26:103101, 2016.

[132] A. Pikovsky and M. Rosenblum. Partially integrable dynamics of hierarchical populations of coupled oscillators. *Phys. Rev. Lett.*, 101:264103, 2008.

[133] A. Pikovsky and M. Rosenblum. Dynamics of globally coupled oscillators: Progress and perspectives. *Chaos*, 25:097616, 2015.

[134] N. C. Rattenborg, C. J. Amlaner, and S. L. Lima. Behavioral, neurophysiological and evolutionary perspectives on unihemispheric sleep. *Neurosci. Biobehav. Rev.*, 24:817–842, 2000.

[135] A. Röhm, F. Böhm, and K. Lüdge. Small chimera states without multistability in a globally delay-coupled network of four lasers. *Phys. Rev. E*, 94:042204, 2016.

[136] D. P. Rosin, D. Rontani, N. D. Haynes, E. Schöll, and D. J. Gauthier. Transient scaling and resurgence of chimera states in networks of Boolean phase oscillators. *Phys. Rev. E*, 90:030902, 2014.

[137] A. Rothkegel and K. Lehnertz. Irregular macroscopic dynamics due to chimera states in small-world networks of pulse-coupled oscillators. *New J. Phys.*, 16:055006, 2014.

[138] J. Sawicki, I. Omelchenko, A. Zakharova, and E. Schöll. Chimera states in complex networks: interplay of fractal topology and delay. *Eur. Phys. J. Special Topics*, 226:1883–1892, 2017.

[139] A. Schmidt, T. Kasimatis, J. Hizanidis, A. Provata, and P. Hövel. Chimera patterns in two-dimensional networks of coupled neurons. *Phys. Rev. E*, 95:032224, 2017.

[140] L. Schmidt, K. Schönleber, K. Krischer, and V. García-Morales. Coexistence of synchrony and incoherence in oscillatory media under nonlinear global coupling. *Chaos*, 24:013102, 2014.

[141] L. Schmidt and K. Krischer. Chimeras in globally coupled oscillatory systems: From ensembles of oscillators to spatially continuous media. *Chaos*, 25:064401, 2015.

[142] L. Schmidt and K. Krischer. Clustering as a prerequisite for chimera states in globally coupled systems. *Phys. Rev. Lett.*, 114:034101, 2015.

[143] E. Schöll. Synchronization patterns and chimera states in complex networks: Interplay of topology and dynamics. *Eur. Phys. J. Special Topics*, 225:891–919, 2016.

[144] V. Semenov, A. Zakharova, Y. Maistrenko, and E. Schöll. Delayed-feedback chimera states: Forced multiclusters and stochastic resonance. *Europhys. Letters*, 115:10005, 2015.

[145] N. Semenova, A. Zakharova, V. Anishchenko, and E. Schöll. Coherence-resonance chimeras in a network of excitable elements. *Phys. Rev. Lett.*, 117:014102, 2016.

[146] G. C. Sethia, A. Sen, and F. M. Atay. Clustered chimera states in delay-coupled oscillator systems. *Phys. Rev. Lett.*, 100:144102, 2008.

[147] G. C. Sethia, A. Sen, and J. L. Johnston. Amplitude-mediated chimera states. *Phys. Rev. E*, 88:042917, 2013.

[148] G. C. Sethia and A. Sen. Chimera states: The existence criteria revisited. *Phys. Rev. Lett.*, 112:144101, 2014.

[149] J. H. Sheeba, V. K. Chandrasekar, and M. Lakshmanan. Chimera and globally clustered chimera: Impact of time delay. *Phys. Rev. E*, 81:046203, 2010.

[150] J. Shena, J. Hizanidis, V. Kovanis, and G. P. Tsironis. Turbulent chimeras in large semiconductor laser arrays. *Sci. Reports*, 7:42116, 2017.

[151] S. Shima and Y. Kuramoto. Rotating spiral waves with phase-randomized core in nonlocally coupled oscillators. *Phys. Rev. E*, 69:036213, 2004.

[152] J. Sieber, O. E. Omel'chenko, and M. Wolfrum. Controlling unstable chaos: Stabilizing chimera states by feedback. *Phys. Rev. Lett.*, 112:054102, 2014.

[153] L. Smirnov, G. Osipov, and A. Pikovsky. Chimera patterns in the Kuramoto-Battogtokh model. *J. Phys. A: Math. Theor.*, 50:08LT01, 2017.

[154] B. Sonnenschein and L. Schimansky-Geier. Onset of synchronization in complex networks of noisy oscillators. *Phys. Rev. E*, 85:051116, 2012.

[155] B. Sonnenschein and L. Schimansky-Geier. Approximate solution to the stochastic Kuramoto model. *Phys. Rev. E*, 88:052111, 2013.

[156] S. H. Strogatz. From Kuramoto to Crawford: exploring the onset of synchronization in populations of coupled oscillators. *Physica D*, 143:1–20, 2000.

[157] Y. Suda and K. Okuda. Persistent chimera states in nonlocally coupled phase oscillators. *Phys. Rev. E*, 92:060901, 2015.

[158] M. R. Tinsley, S. Nkomo, and K. Showalter. Chimera and phase-cluster states in populations of coupled chemical oscillators. *Nature Phys.*, 8:662–665, 2012.

[159] J. F. Totz, R. Snari, D. Yengi, M. R. Tinsley, H. Engel, and K. Showalter. Phase-lag synchronization in networks of coupled chemical oscillators. *Phys. Rev. E*, 92:022819, 2015.

[160] N. D. Tsigkri-DeSmedt, J. Hizanidis, P. Hövel, and A. Provata. Multi-chimera states and transitions in the Leaky Integrate-and-Fire model with nonlocal and hierarchical connectivity. *Eur. Phys. J. Special Topics*, 225:1149–1164, 2016.

[161] S. R. Ujjwal and R. Ramaswamy. Chimeras with multiple coherent regions. *Phys. Rev. E*, 88:032902, 2013.

[162] S. Ulonska, I. Omelchenko, A. Zakharova, and E. Schöll. Chimera states in networks of Van der Pol oscillators with hierarchical connectivities. *Chaos*, 26:094825, 2016.

[163] A. Vüllings, J. Hizanidis, I. Omelchenko, and P. Hövel. Clustered chimera states in systems of type-I excitability. *New J. Phys.*, 16:015103, 2014.

[164] S. Watanabe and S. H. Strogatz. Integrability of a globally coupled oscillator array. *Phys. Rev. Lett.*, 70:2391, 1993.

[165] S. Watanabe and S. H. Strogatz. Constants of motion for superconducting Josephson arrays. *Physica D*, 74:197–253, 1994.

[166] M. Wickramasinghe and I. Z. Kiss. Spatially organized dynamical states in chemical oscillator networks: Synchronization, dynamical differentiation, and chimera patterns. *PLoS ONE*, 8:e80586, 2013.

[167] M. Wickramasinghe and I. Z. Kiss. Spatially organized partial synchronization through the chimera mechanism in a network of electrochemical reactions. *Phys. Chem. Chem. Phys.*, 16:18360, 2014.

[168] D. A. Wiley, S. H. Strogatz, and M. Girvan. The size of the sync basin. *Chaos*, 16:015103, 2006.

[169] J. Wojewoda, K. Czolczynski, Y. Maistrenko, and T. Kapitaniak. The smallest chimera state for coupled pendula. *Sci. Reports*, 6:34329, 2016.

[170] M. Wolfrum, O. E. Omel'chenko, S. Yanchuk, and Y. L. Maistrenko. Spectral properties of chimera states. *Chaos*, 21:013112, 2011.

[171] M. Wolfrum and O. E. Omel'chenko. Chimera states are chaotic transients. *Phys. Rev. E*, 84:015201, 2011.

[172] M. Wolfrum, O. E. Omel'chenko, and J. Sieber. Regular and irregular patterns of self-localized excitation in arrays of coupled phase oscillators. *Chaos*, 25:053113, 2015.

[173] M. Wolfrum, S. V. Gurevich, and O. E. Omel'chenko. Turbulence in the Ott-Antonsen equation for arrays of coupled phase oscillators. *Nonlinearity*, 29:257–270, 2016.

[174] J. Xie, E. Knobloch, and H.-C. Kao. Multicluster and traveling chimera states in nonlocal phase-coupled oscillators. *Phys. Rev. E*, 90:022919, 2014.

[175] J. Xie, E. Knobloch, and H.-C. Kao. Twisted chimera states and multicore spiral chimera states on a two-dimensional torus. *Phys. Rev. E*, 92:042921, 2015.

[176] J. Xie, H.-C. Kao, and E. Knobloch. Chimera states in systems of nonlocal nonidentical phase-coupled oscillators. *Phys. Rev. E*, 91:032918, 2015.

[177] N. Yao, Z.-G. Huang, Y.-C. Lai, and Z.-G. Zheng. Robustness of chimera states in complex dynamical systems. *Sci. Reports*, 3:3522, 2013.

[178] N. Yao, Z.-G. Huang, C. Grebogi, and Y.-C. Lai. Emergence of multicluster chimera states. *Sci. Reports*, 5:12988, 2015.

[179] N. Yao and Z. Zheng. Chimera states in spatiotemporal systems: Theory and applications. *Int. J. Mod. Phys. B*, 30:1630002, 2016.

[180] A. Yeldesbay, A. Pikovsky, and M. Rosenblum. Chimera-like states in an ensemble of globally coupled oscillators. *Phys. Rev. Lett.*, 112:144103, 2014.

[181] A. Zakharova, M. Kapeller, and E. Schöll. Chimera death: Symmetry breaking in dynamical networks. *Phys. Rev. Lett.*, 112:154101, 2014.

[182] M. Zaks and A. Pikovsky. Chimeras and complex cluster states in arrays of spin-torque oscillators. *Sci. Reports*, 7:4648, 2017.

[183] Y. Zhu, Y. Li, M. Zhang, and J. Yang. The oscillating two-cluster chimera state in non-locally coupled phase oscillators. *Europhys. Lett.*, 97:10009, 2012.

[184] Y. Zhu, Z. Zheng, and J. Yang. Chimera states on complex networks. *Phys. Rev. E*, 89:022914, 2014.